REVIEW

Advances in depressants used for pyrite flotation separation from coal/minerals

Yulong Li[1] · Gan Cheng[1,2,3] · Mengni Zhang[1] · Yijun Cao[4] · Ee Von Lau[5]

Abstract

Pyrite is separated from other minerals mainly by flotation. However, the hydrophilicity of pyrite is affected by many factors, causing it to easily enter the concentrate and consequently reduce the quality of concentrate. Highly efficient pyrite depressants can be selectively adsorbed on the surface of pyrite to improve its hydrophilicity, thereby increasing the flotation separation efficiency. Understanding the fundamental inhibition mechanism of depressants on pyrite is a prerequisite to improve the flotation desulfurization efficiency. The inhibition ability and mechanism of different types of pyrite depressants are reviewed in this manuscript. In recent years, molecular simulation has increasingly become a powerful tool to study the interaction between reagents and minerals, shedding new light on the adsorption mechanisms of reagents on mineral surfaces at the atomic and electronic levels. The properties of sulfide mineral and flotation reagents as well as the microscopic adsorption mechanistic studies of reagents on mineral surfaces based on quantum chemistry and molecular simulation are also reviewed.

Keywords Pyrite · Flotation · Depressant · Coal · Mineral

1 Introduction

Pyrite (FeS_2), one of the most common sulfide minerals, is not only associated with coal and nonferrous metals (chalcopyrite, galena, and sphalerite) (Wang and Forssberg 1991), but also it is the primary carrier of some precious metals such as gold and silver (Bi et al. 2020). Existence of pyrite in minerals and coal greatly affects their quality (Mu et al. 2016b). Furthermore, oxidation of pyrite in the tailings is one of the main reasons for the formation of acid mine wastewater (AMD) (Chen et al. 2014b; Bai et al. 2021).

✉ Gan Cheng
  chenggan464@126.com

1 College of Chemistry and Chemical Engineering, Henan Polytechnic University, Jiaozuo 454000, China

2 Henan Key Laboratory of Coal Green Transformation, Henan Polytechnic University, Jiaozuo 454000, China

3 Collaborative Innovation Center of Coal Work Safety and Clean High Efficiency Utilization, Henan Polytechnic University, Jiaozuo 454000, China

4 School of Chemical Engineering, Zhengzhou University, Zhengzhou 450000, China

5 School of Engineering, Monash University Malaysia, Selangor 47500, Malaysia

China has abundant coal reserves (Li et al. 2020). The coal reserves in China were estimated at 138.819 billion tons in 2018, accounting for 13.2% of the world's total coal reserves (Cheng et al. 2019a, 2020a, b). The range of sulfur content in various grades of coal is shown in Table 1; the proportions of medium-high sulfur coal and high sulfur coal are 7% and 3%, respectively (Tang et al. 2015). Sulfur in coal can be classified into inorganic sulfur and organic sulfur. Inorganic sulfur mainly exists in the form of sulfide minerals (mainly pyrite), accompanied by a small amount of sulfate. On the other hand, thiophene (C_4H_4S), organic disulfide (R–S–S–R), thiol (–SH), and thioether (R–S–R) are the main forms of organic sulfur (Xu et al. 2021; Xiong et al. 2020). Pyrite accounts for about 60%–70% of the total sulfur in high-sulfur coal (Wang 2013). The main forms of pyrite in coal are finely dispersed pyrite, large blocks of pyrite, invaded pyrite, and stuffed pyrite (Yu 2013). In China, about 80% of coal is used as fuel (Tao et al. 2014), producing gaseous SO_2 when burnt (DeCuir et al. 2021). This gaseous SO_2 then easily causes acid rain (Cheng et al. 2019c), which pollutes the environment, damages buildings, as well as accelerates the corrosion of metal parts such as boilers and pipelines (Cheng and Zhang 2018). In addition, the conversion of SO_2 from gaseous to solid state also contributes to the formation of PM2.5 (Xu et al. 2021). Coal with a high

Table 1 Sulfur content in various grades of coal

Grade	$S_{t, d}$ (%)
Ultralow sulfur coal	≤ 0.50
Low sulfur coal	0.51–1.00
Low-medium sulfur coal	1.01–1.50
Medium sulfur coal	1.51–2.00
Medium-high sulfur coal	2.01–3.00
High sulfur coal	> 3.00

pyrite content is also known to promote the oxidation and spontaneous combustion of coal, thus triggering transportation security risks.

Pyrite is often distributed in rock in the form of blocks or filled along the cracks of rock in the form of veins. Particle size distribution of pyrite is generally within the range of 0.3–0.5 mm, mainly associated with chalcopyrite, galena, and sphalerite (Liu and Zhou 2016). Strawberry-shaped pyrite in manganese is composed of multiple pyrite berries and formed during the formation of manganese ore, whereas euhedral-semi-automatic pyrite and pyrite beds formed during the diagenesis exist in manganese-bearing rocks (Wang et al. 2016).

Because of different formation conditions of coal-derived pyrite (coal pyrite for short) and ore-related pyrite (ore pyrite for short), their physicochemical properties are vastly different. Xi et al. (2016) assumed that the S atoms were replaced with C atoms in coal pyrite. In addition, the S/Fe molar ratio of ore pyrite is 1.96:1, close to the standard S/Fe molar ratio (2:1), and the C content is only 6.82%. On the other hand, the S/Fe molar ratio of coal pyrite is 1.85:1, and the C content reaches 19.46% (Yu 2013). Therefore, a part of S atoms might be replaced with C atoms in coal pyrite. However, the existence of C in coal pyrite is complex, where C atoms might exist in the form of C–Fe compounds (Shao et al. 1994). Xu (2018) compared the magnetic susceptibility and thermal stability of coal pyrite and ore pyrite. The magnetic values of coal pyrite and ore pyrite reached the maximum at 500 °C and 550 °C, respectively. In other words, ore pyrite required a higher temperature to achieve stronger magnetic properties compared to coal pyrite. In addition, coal pyrite had a lower pyrolysis temperature and greater maximum weight loss than those of ore pyrite, indicating that the existence of organic matter in coal pyrite affected its pyrolysis.

The separation difficulties of coal pyrite and ore pyrite are different due to the difference in their physicochemical properties. Xi et al. (2016) showed that the hydrophobicity of coal pyrite is higher due to the substitution of C. In addition, finely dispersed pyrite is embedded in coal and coexists with coal in the form of coal pyrite conjoined body. Cao et al. (2019) found that the content of coal pyrite bodies was far higher than that of coal and pyrite monomers in raw coal despite it being ground for 150 s. Therefore, the coexistence of coal and pyrite is the main factor affecting their separation.

Doped atoms (Co, Ni, Cu, Au, Sb) often exist in pyrite, leading to higher surface oxidation activity and floatability, larger unit cell, and lower pyrite hardness (Tu 2017). Besides, pyrite floatability is also affected by its activation, oxidation, single-crystal morphology, lattice defects, impurity types, and content. For example, pyrite containing Au, Ni, Co, and C atoms has better floatability (Xian 2013).

As one of the most commonly used sulfide mineral collectors (Bulut and Atak 2002; Valdivieso et al. 2005; Yang et al. 2018), xanthate has satisfactory collection efficiency of pyrite. However, it is necessary to suppress pyrite rather than collect pyrite in many cases. Therefore, efficient pyrite depressants play an important role in flotation. Mu et al. (2016b) reviewed widely used pyrite depressants and their interaction mechanisms. In recent years, with the rapid development of theoretical chemistry and computational chemistry, quantum chemistry and molecular simulation have become increasingly powerful tools to study the molecular properties of flotation reagents and reagent/mineral interaction. As such, further review is needed on the advances in pyrite depression in these aspects. Here, based on the commonly used pyrite depressants, recent studies on the surface properties of sulfide minerals, flotation characteristics of reagents, and adsorption of reagents on mineral surfaces are reviewed from the perspective of quantum chemistry and molecular simulation. The advantages of computational simulation and its future development prospects are also analyzed.

2 Oxidation and surface activation pathways of pyrite in solution

Pyrite is easily oxidized in solutions, affecting the adsorption of collectors on its surface (Huang et al. 2013; Niu et al. 2019). Oxidation extent of S atom in pyrite is closely related to pulp pH. When the pH is less than 6, elemental sulfur (S^0) is the main existing form of S atom; with the increase in pH, S^0 gradually oxidizes to SO_4^{2-} (Niu et al. 2019). The hydrophobicity of pyrite is enhanced by S^0 and polysulfide (S_n^{2-}), while SO_4^{2-} and SO_3^{2-} exhibit better hydrophilicity (Huang et al. 2013). Therefore, an alkaline environment is preferred for the depression of pyrite (Bulut et al. 2011; Sarquís et al. 2014). Reactions involved in the oxidation of pyrite are as follows (Liu et al. 2020a):

$$FeS_2 + 11H_2O - 15e^- \rightarrow Fe(OH)_3 + 2SO_4^{2-} + 19H^+ \quad (1)$$

$$O_2 + 4e^- + 4H^+ \rightarrow 2H_2O \quad (2)$$
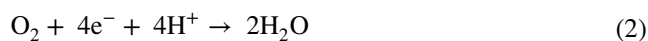
Shi et al. (1997) reported that unoxidized and highly oxidized pyrite had preferable hydrophilicity. Jin et al. (2015) studied the effect of oxidation on the interfacial water structure on pyrite surface. Hydrogen bonds and electrostatic attraction between $Fe(OH)_3$ and H_2O increased the wettability of pyrite. Here, Fe(III) might be adsorbed on pyrite surface as $Fe(OH)^{2+}$ and $Fe(OH)_2^+$ (Yang et al. 2018). The concentration of these Fe-containing substances adsorbed on pyrite surface was dependent on the oxidation degree of pyrite (Fairthorne et al. 1997). On a different note, Cu dissolves from the chalcopyrite lattice, leaving a metal-deficient sulfur-rich surface, which is then readsorbed or precipitated as hydroxide species on the chalcopyrite surface. The hydrophobicity and flotation performance of chalcopyrite are as such dependent on oxidation processes, i.e., metal dissolution that produces a hydrophobic surface and metal hydroxide precipitation that produces a hydrophilic surface (Fairthorne et al. 1997).

In a different manner, pyrite could be surface activated by the Cu atoms present in pulp. Cu^{2+} adsorbed on the pyrite surface undergoes an immediate redox reaction with S^{2-} to generate Cu^+ and S^-; at the same time, Fe^{2+} is oxidized to Fe^{3+} by S^-, which then reduces to S^{2-} (Fig. 1) (Fletcher et al. 2020). After being activated by Cu^{2+}, the surface potential of pyrite changes from positive to negative; this potential was observed to be close to that of $CuFeS_2$. Chalcopyrite ($CuFeS_2$) layers might have formed on the pyrite surface (Ejtemaei and Nguyen 2017). $CuFeS_2$ easily interacts with xanthate or oil collectors, improving the floatability of pyrite under alkaline conditions (Fletcher et al. 2020). In addition, Cu activation of sphalerite occurs in two steps: (1) substitution of Zn^{2+} with Cu^{2+} and (2) oxidation of S^{2-} to S^- by the reduction of Cu^{2+} to Cu^+, followed by a CuS-type layer formation on the mineral surface. The zeta potential of copper-activated sphalerite showed almost similar zeta potential as that of CuS (Fletcher et al. 2020). Thus, the floatability of sphalerite is affected by the concentration of copper. At low copper concentrations, sphalerite flotation increased due to the formation of a sulfur-rich surface, following copper adsorption (as Cu^{2+} or $Cu(OH)_2$), its exchange with zinc at the surface and in the sphalerite lattice, and the reduction of cupric sulfide to cuprous sulfide with the oxidation of sulfide to polysulfide; at higher copper concentrations, above the solubility limit of $Cu(OH)_2$ and in the pH range 7–11, copper hydroxide started to precipitate on the polysulfide surface and depressed sphalerite flotation (Fornasiero and Ralston 2006).

3 Pyrite depressants and their mechanism

3.1 Coal pyrite depressants

Although the contact angle is smaller and the induction time of coal pyrite is longer than those of coal (Qi et al. 2019), coal pyrite has better floatability than ore pyrite due to the doping of C atoms. Efficient depressants are needed to inhibit the floatability of pyrite in the flotation separation of coal and pyrite. Liu and Wu (2015) noted that the desulfurizing efficiency of thioglycolic acid (TGA) depressant is higher than that of vitamin C and lime. Shao et al. (1997) reported that the Fe sites of pyrite (active adsorption areas of xanthate) were occupied by the SH group of TGA. Furthermore, the negative charge of coal pyrite surface was enhanced by TGA, which caused electrostatic repulsion between pyrite and coal. The depression performance of other depressants decreased in the following order: tannic acid (TA) > sodium humate (NaA) > pyrogallol > calcium hypochlorite > starch (Yu 2013). Although TA and NaA exhibited good performance by reducing the hydrophobicity of pyrite, they induced strong corrosion and depression effects on clean coal, therefore rendering them unsuitable for the floatability of clean coal.

Both strong oxidants and reductants can be used as depressants, but oxidants might cause the loss of clean coal. Shi et al. (1997) reported that the reductant $C_6H_3(OH)_3$ effectively depressed coal pyrite by lowering the pulp potential or forming hydrophilic complexes with Fe ions on the mineral surface. Sotillo et al. (1997) reported that hydrophilic complexes formed by the reaction between TEPA ($(NH_2)_2^+CSC_2H_4PO(OH)O^-$) and the Fe atoms of pyrite as a new depressant removed a part of pyrite, but had no effect on ash removal rate. On a different note, H_2O_2 is the most common oxidant for desulfurization and can provide good sulfur removal rate (Pecina et al. 2012); however, it causes environmental pollution.
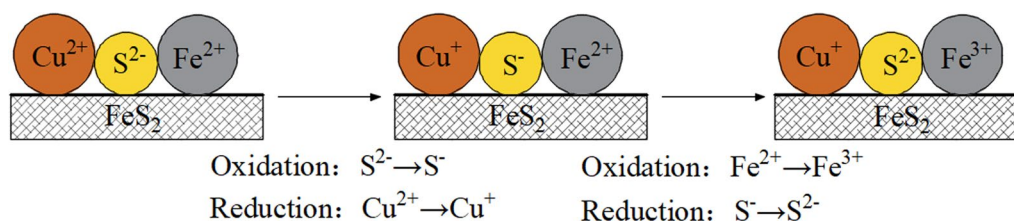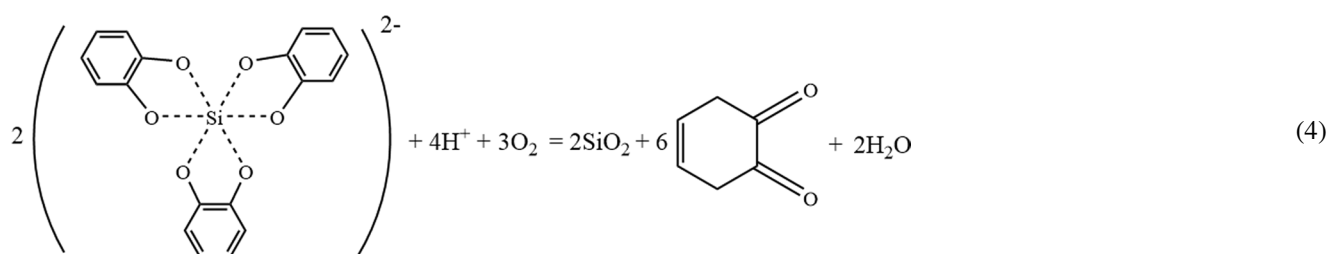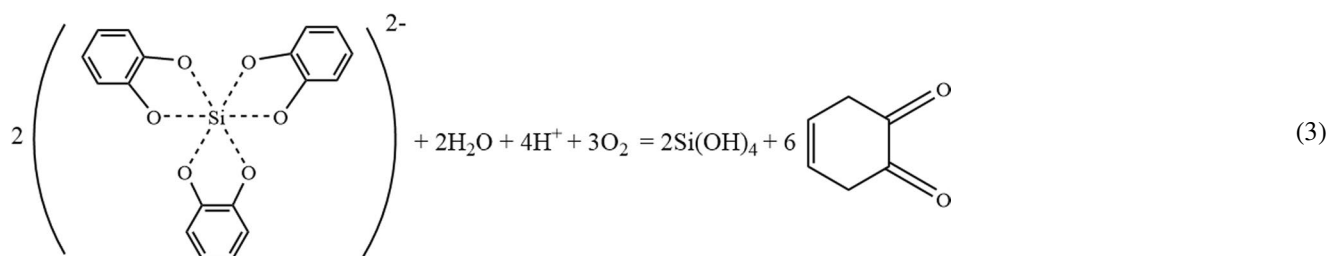

Fig. 1 Surface activation of pyrite by Cu.$^{2+}$. Modified with permission from Ejtemaei and Nguyen (2017)

In addition, H_2O_2 might also have destructive effect on coal quality. Therefore, when oxidants or reductants are used to assist desulfurization, the recovery of these reagents should be considered.

Recently, carrier-microencapsulation (CME) technology has been developed (Jha et al. 2011, 2008; Satur et al. 2007). The mechanism of CME is that when organic carriers (such as catechol) and metal ions (such as Ti^{4+} and Si^{4+}) are added to the pulp, coordination compounds are formed on the mineral surface. The organic carrier is then oxidized and decomposed, and hydrophilic metal oxide/hydroxide layers are formed by the released metal ions. Jha et al. (2011) reported that the synthesized coordination compound $Si(cat)_3^{2-}$ formed hydrophilic SiO_2 and $Si(OH)_4$ on pyrite surface (Eqs. (3) and (4)). Nonetheless, $Si(cat)_3^{2-}$ cannot decompose and form hydrophilic film layers on the coal surface because the conductivity of pyrite and coal is inconsistent.

3.2 Ore- pyrite depressants

Although xanthate is one of the most commonly used collector for sulphide ores, its substantial adsorption on sulfide surface limits its potential and advocates the exploration of new sulfide ore collectors and depressants. The collecting mechanism of xanthate for pyrite can be explained as follows: Metal hydroxides (oxidation product of pyrite) and xanthate ions (X^-) are subjected to redox reactions, generating hydrophobic dixanthogen (X_2) on the pyrite surface. Moreover, the content of hydrophilic iron hydroxide decreases, leading to an increase in the floatability of pyrite (Bulut and Atak 2002; Valdivieso et al. 2005). The collection mechanism of xanthate for pyrite is shown in Fig. 2. Hydrophobic ferric hydroxo-xanthate layers may be formed on pyrite surface due to the chemisorption between xanthate ions and $Fe(OH)_2^+$, $Fe(OH)^{2+}$, and pyrite clusters; the adsorption process is thermodynamically feasible (Ejtemaei

$$2 \left(\text{Si(cat)}_3 \right)^{2-} + 2H_2O + 4H^+ + 3O_2 = 2Si(OH)_4 + 6 \text{ (benzoquinone)} \tag{3}$$

$$2 \left(\text{Si(cat)}_3 \right)^{2-} + 4H^+ + 3O_2 = 2SiO_2 + 6 \text{ (benzoquinone)} + 2H_2O \tag{4}$$

Besides, the separation of coal and pyrite is also affected by the mechanical entrainment of foams and mutual affinity in flotation (Fornasiero and Ralston 2006; Wang 2013). Qi et al. (2019) reported that dodecane collector could not penetrate the hydration film on pyrite surface. Consequently, pyrite persisted in clean coal due to the entrainment of foam. The positive charge of coal increased because of the adsorption of pyrite, further decreasing the separation efficiency (Fornasiero and Ralston 2006). Although many factors affect the effective separation of coal and pyrite, the degree of coal and pyrite dissociation in grinding and the entrainment of foam in flotation are the main influencing factors.

and Nguyen 2017). Therefore, effective pyrite depressants are both capable of adsorbing pyrite to improving the hydrophilicity, as well as preventing the formation of hydrophobic dixanthogen.

3.2.1 Inorganic depressants

Cyanide is one of the most common inorganic depressants in the separation of sulfide minerals (Guo et al. 2014; Zhao et al. 2016). Cyanide produces ferricyanide or reduces the electrochemical activity of minerals to prevent the
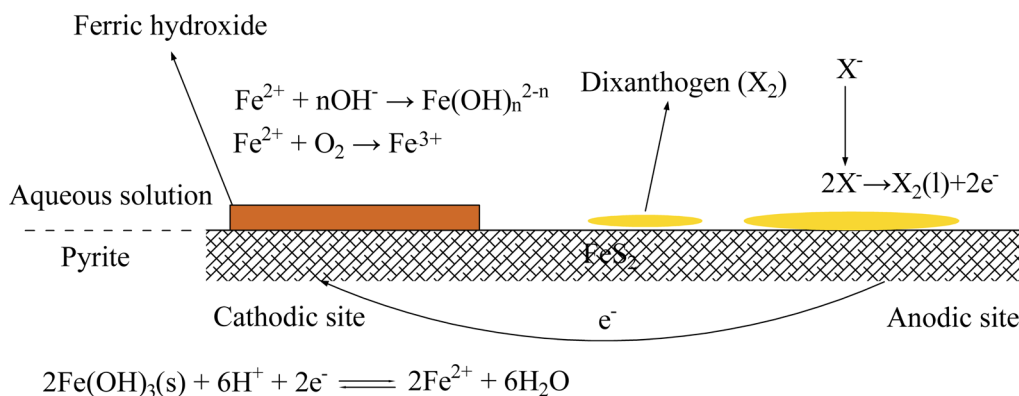
Ferric hydroxide

$$Fe^{2+} + nOH^- \rightarrow Fe(OH)_n^{2-n}$$
$$Fe^{2+} + O_2 \rightarrow Fe^{3+}$$

Dixanthogen (X_2) X^-

Aqueous solution

$$2X^- \rightarrow X_2(l) + 2e^-$$

Pyrite FeS_2

Cathodic site e^- Anodic site

$$2Fe(OH)_3(s) + 6H^+ + 2e^- \rightleftharpoons 2Fe^{2+} + 6H_2O$$

Fig. 2 Collection mechanism of xanthate ions. Modified with permission from Valdivieso et al. (2005)

ADD   ADD   ADD

FeS_2 ADD $\longrightarrow$ FeS_2

(a) Pyrite   (b) ADD adsorption on pyrite

$Ca(ClO)_2$

$Fe(OH)_3$ $CaSO_4$ $Ca(OH)^+$ $Fe(OH)_3$ ADD $CaSO_4$ $Ca(OH)^+$

FeS_2 ADD $\longrightarrow$ FeS_2

(c)   Passivation of pyrite   (d)   Depression of ADD adsorption
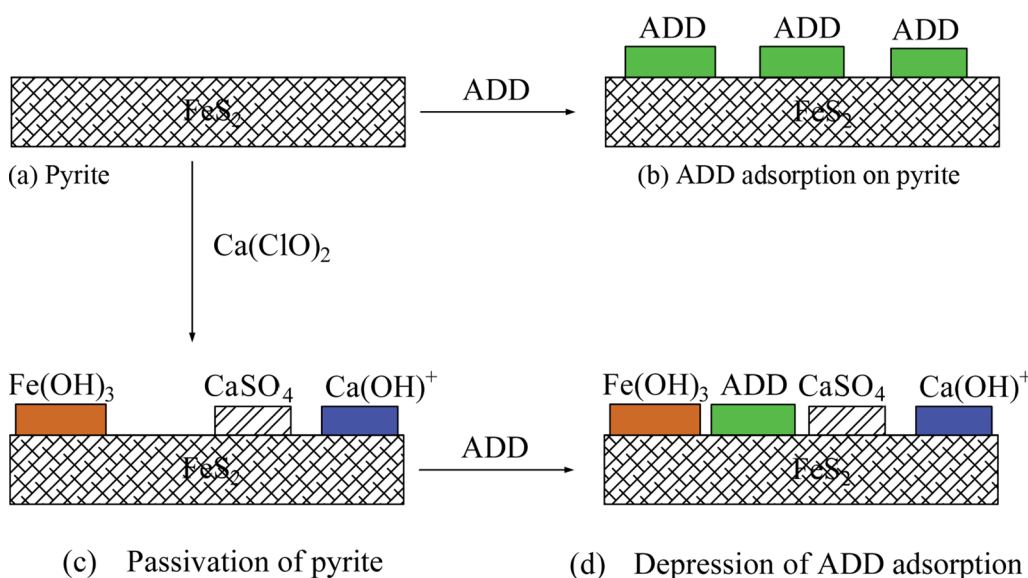
Fig. 3 Depression mechanism of $Ca(ClO)_2$ for pyrite. Modified with permission from Yin et al. (2019)

adsorption and oxidation of xanthate (Guo et al. 2014). Guo et al. (2016) reported that the redox potential of pyrite was reduced due to the adsorption of cyanide; however, this reduction was insignificant in hindering the adsorption of xanthate and formation of dixanthogen. As a result, $Fe(CN)_n^{m-}$ ($n < 6$) was produced by the reaction of CN^- and Fe atoms (Zhu et al. 2013). Wang and Forssberg (1996) reported that $Fe(CN)_6^{4-}$ and $Fe(CN)_6^{3-}$ are the main products in the Fe-CN-Xanthate-H_2O system under neutral to alkaline conditions; as such, the reactivity between xanthate and passivated pyrite might be reduced due to the passivation effect of $Fe(CN)_n^{m-}$ on pyrite (Guo et al. 2016).

The properties of pyrite surface are easily affected by oxidants. Hydrophobic cuprous-xanthate complexes are instantaneously formed on copper-activated pyrite surface; then, they are further oxidized with sodium sulfite to produce hydrophilic

copper hydroxide (Shen et al. 2001). Hydrophilic Fe–O/OH was formed upon the oxidation of pyrite with H_2O_2, which provided more adsorption sites for dextrin depressant (Bogusz et al. 1997). Yin et al. (2019) reported that at pH 10, the residual potential of pyrite surface was 0.01 V, and FeS_2 oxidized with $Ca(ClO)_2$ to form $CaSO_4$ and $Fe(OH)_3$ precipitates, which inhibited the adsorption of collector ammonium dibutyl dithiophosphate (ADD). Furthermore, the electronegativity of pyrite also decreased due to the adsorption of $Ca(OH)^+$. The depression mechanism of $Ca(ClO)_2$ is shown in Fig. 3; similar results have been reported by other researchers (Bai et al. 2019).

Alkaline conditions are beneficial to the hydroxylation of metal atoms on pyrite surface. Iron hydroxyl generated from OH^- and Fe hindered the adsorption of xanthate and desorbed xanthate ions (Li et al. 2012). Zhang et al. (2011) reported that the depression ability of lime is stronger than

that of sodium hydroxide, as lime formed hydrophilic calcium films on pyrite surface. Interestingly, lime and sodium hydroxide are also known as pH modifiers as they reduce the floatability of pyrite, mainly by changing the pulp pH. Ca^{2+} plays an important role in the depression of pyrite; the depression mechanism of Ca^{2+} will be further discussed in Sect. 4.

3.2.2 Organic depressants

The main disadvantages of inorganic reagents are their toxicity, corrosiveness, and nondegradability, which are harmful to the environment. As such, nontoxic, renewable, and readily biodegradable natural polysaccharides such as starch, dextrin, guar gum and carboxymethyl cellulose (CMC) were evaluated as pyrite depressants (Bulut et al. 2011; Fletcher et al. 2020). The main factors that influence the properties of organic depressants are molecular structure, type of functional group, polymer molecular conformation, and pulp pH. For instance, depressants that contain sulfonic acid groups or benzene rings have substantial adsorption ability on pyrite (Chen et al. 2010; Sun et al. 2005). On the other hand, the hydroxylation of mineral surface, dissociation of carboxyl groups, and stability of $Fe(OH)_3$ layers could be affected by pulp pH (Bicak et al. 2007; Rath et al. 2000).

3.2.2.1 Polysaccharide depressants Natural polysaccharides are macromolecular polymers, and they are composed of different monosaccharides (Liu and Laskowski 1989). Polysaccharides can form hydrophilic layers on pyrite surface by interacting with hydroxylated metals, and they slightly affect the conversion of xanthate to dixanthogen. As such, coadsorption might occur between xanthate and polysaccharides on the mineral surface (Mu et al. 2016b).

Starch is widely used as a depressant in the flotation of sulfide minerals owing to its wide availability, low cost, and nontoxicity. Han et al. (2019b) reported that new characteristic peaks appeared after pyrite was treated with starch, indicating that both physical adsorption and chemical adsorption occurred simultaneously. Fletcher et al. (2020) reported that the depression ability of oxidized starch is stronger than that of ordinary starch. Experimental results showed that the recovery of pyrite was 4.0% when the dosage of ordinary starch was 700 g/t, while the recovery of pyrite was only 2.0% when the dosage of oxidized starch was 500 g/t.

Dextrin is a product of partial thermal degradation of starch under acidic conditions (Mu et al. 2016b). As the adsorption of dextrin requires the presence of metal oxides on pyrite surface, dextrin can therefore be adsorbed on pyrite surface when pyrite is oxidized or doped with metal ions (Bogusz et al. 1997). The surface properties of oxidized pyrite are complex, where Fe(III)–O/OH compounds are the known adsorption sites of dextrin, and the adsorption

amount of dextrin is directly proportional to the concentration of Fe(III)–O/OH. Besides Fe(III)–O/OH, Fe(II)–OH was also identified as the adsorption site of dextrin (Valdivieso et al. 2004). As xanthate tends to be adsorbed on the unoxidized anode sites of pyrite, the adsorption of dextrin was satisfactory at pH higher than 4 (Valdivieso et al. 2007). Valdivieso et al. (2004) reported that the redox reactions between xanthate ion and ferric hydroxide generated hydrophobic dixanthogen and reduced the concentration of ferric hydroxide, resulting in the desorption of dextrin and pyrite. However, because the oxidation of pyrite could be accelerated by blowing air into the pulp, the number of adsorption sites of dextrin increased.

Cationic guar gum is a water-soluble polymer; the hydroxyl groups of guar gum can be adsorbed with iron hydroxide ions ($Fe(OH)_2^+$, $Fe(OH)^{2+}$) under alkaline conditions. Hydrogen bonds and Bronsted acid–base interactions are the main driving forces for the adsorption of guar gum on pyrite surface. The molecular weight had no effect on its inhibiting ability (Bicak et al. 2007).

Modified polysaccharides were synthesized by introducing other functional groups to polysaccharides via etherification or esterification reactions (Mu et al. 2016b). CMC is the product of etherification reaction between carboxymethyl and polysaccharide (Liu and Laskowski 1989); CMC has selective adsorption properties. Unlike guar gum, CMC contains negatively charged carboxyl groups. CMC with a high substitution degree demonstrated low adsorption ability, probably because of the electrostatic repulsion effect between the negatively charged substituents of CMC and negatively charged pyrite surface at pH 9. In this case, CMC modified with Ca^{2+} decreased the negative charge of pyrite surface and promoted the adsorption of CMC (Bicak et al. 2007). Unlike starch and dextrin, CMC and xanthate were competitively adsorbed on pyrite surface (Fig. 4) (Feng et al. 2013; Mu et al. 2016b).

Konjac glucomannan is another natural polysaccharide extracted from amorphophallus konjac. Liu et al. (2020a) compared the abilities of konjac glucomannan, starch, guar gum, and dextrin in the flotation separation of chalcopyrite and pyrite. Figure 5 shows that with the increase in depressant dosage, the recovery of pyrite and chalcopyrite decreased at varying degrees compared to the depression ability of starch on the two minerals, which was undesirable. When the dosage of konjac glucomannan, guar gum, and dextrin was 10 mg/L, the recovery of pyrite was 2.11%, 27.46%, and 33.68%, respectively; while the recovery of chalcopyrite was 92.06%, 90.05%, and 93.26%, respectively. Konjac glucomannan showed superior selectivity to chalcopyrite and pyrite than starch, dextrin, and guar gum. The depression mechanisms of konjac glucomannan and guar gum are similar owing to their similar molecular structure, i.e., hydrogen bonds between the OH groups of konjac
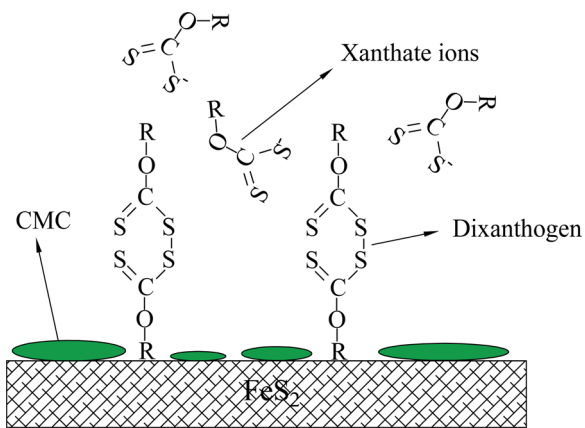
Fig. 4 Competitive adsorption of CMC and xanthate. Modified with permission from Mu et al. (2016b)

glucomannan and $Fe(OH)_3$ are formed through Bronsted acid–base interaction. Furthermore, the oxidation atmosphere of pyrite surface decreased owing to the adsorption of konjac glucomannan, inhibiting the conversion of xanthate to dixanthogen.

Chitosan shows excellent selective adsorption performance in binary metal systems (Vold et al. 2003). Huang et al. (2013) reported that the inhibiting ability of chitosan on pyrite, galena, sphalerite, and chalcopyrite varied in pure mineral flotation, while in mixed mineral flotation, it showed selective inhibiting ability. The selective adsorption of chitosan was dependent on the electron affinity of lattice metal ions. The greater the electron affinity of metal ions, the stronger the interaction between metal ions and the amino group of chitosan. The selectivity of chitosan on pyrite is greater than that on galena (Huang et al. 2013).

Recently, a polysaccharide–metal cyclic complex was observed to be formed when both the hydroxyl groups in a polysaccharide molecule lost a proton according to the Brønsted–Lowry acid–base theory. This complex is capable of enhancing the adsorption properties of polysaccharides (Eq. (5)) (Laskowski et al. 2007; Liu et al 2000).
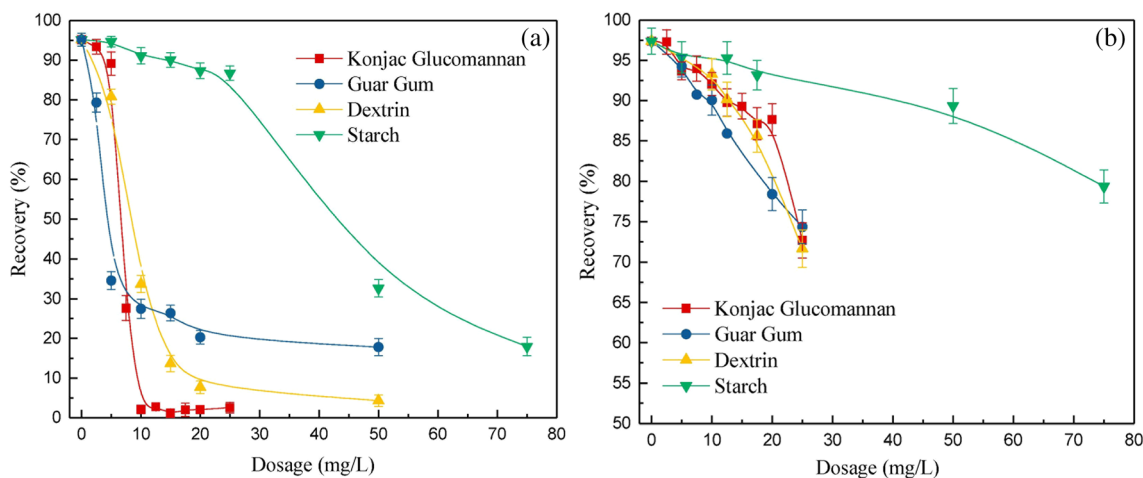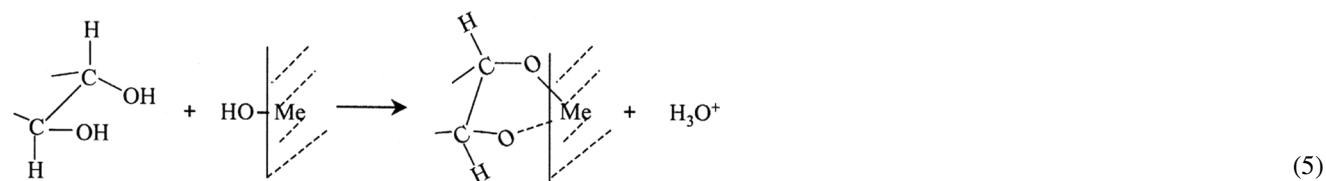

$$\tag{5}$$

Fig. 5 Effect of dosage of depressants on the recovery of **a** Pyrite and **b** Chalcopyrite under different reagent conditions (pH = 9.0, c (xanthate) = 9.5 mg/L). Reprinted with permission from Liu et al. (2020a)
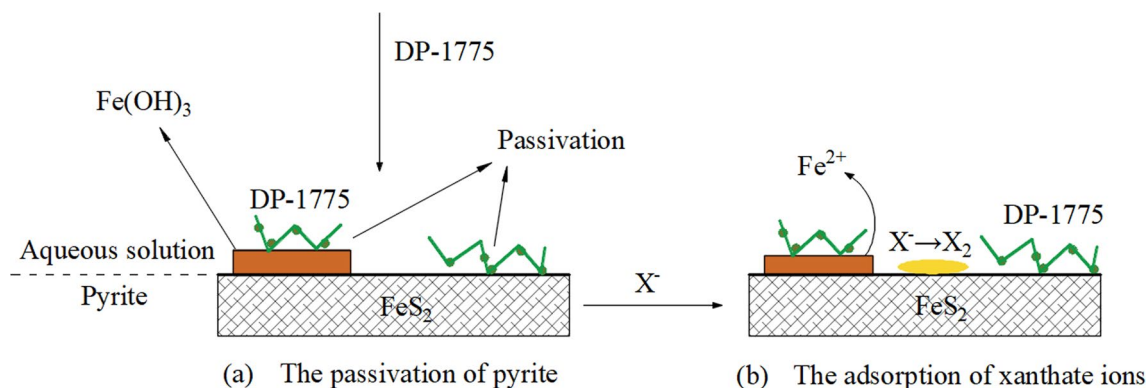
Fig. 6 Adsorption of xanthate ions and biopolymer on pyrite surface. Modified with permission from Mu et al. (2015)

3.2.2.2 Lignosulfonate depressants Lignosulfonate, also known as sulfonated lignin, is a byproduct of sulfite papermaking pulp (Ouyang et al. 2006). Modified lignosulfonate is highly cross-linkable and contains hydrophilic groups such as hydroxyl, sulfonic, and carboxyl groups; these hydrophilic groups are connected with hydrophobic hydrocarbyl group (Ouyang et al. 2010). Liu et al. (2009) reported that calcium lignosulfonate could be adsorbed on the mineral surface and increased the reducibility of mineral through the interactions between SO_3 group and $Fe(OH)_3$. Mu et al. (2015) found that the charge-transfer resistance of pyrite increased with the addition of lignosulfonate depressants (DP-1775), indicating that the oxidation of pyrite was depressed by DP-1775. Besides, the capacitance of pyrite remained constant before and after the adsorption of

DP-1775, suggesting a possibility that both the oxidized and nonoxidized sites of pyrite were occupied by the biopolymer. Figure 6 shows that the adsorption sites of xanthate ion (X^-) were occupied by DP-1775. Owing to the presence of diverse functional groups in lignosulfonate, it might be adsorbed on pyrite through electrostatic attraction, hydrophobic interaction, hydrogen bonding, or chemical bonding (Fig. 7) (Mu et al. 2015; Yekeler and Yekeler 2006).

3.2.2.3 Other organic depressants Other organic depressants include modified biopolymer, TA, polyglutamic acid (PGA), and NaA.

In biopolymers, owing to the formation of heterocyclic rings in their molecular structure, donor atoms and metal ions are easily chelated, and the stability of metal chelate
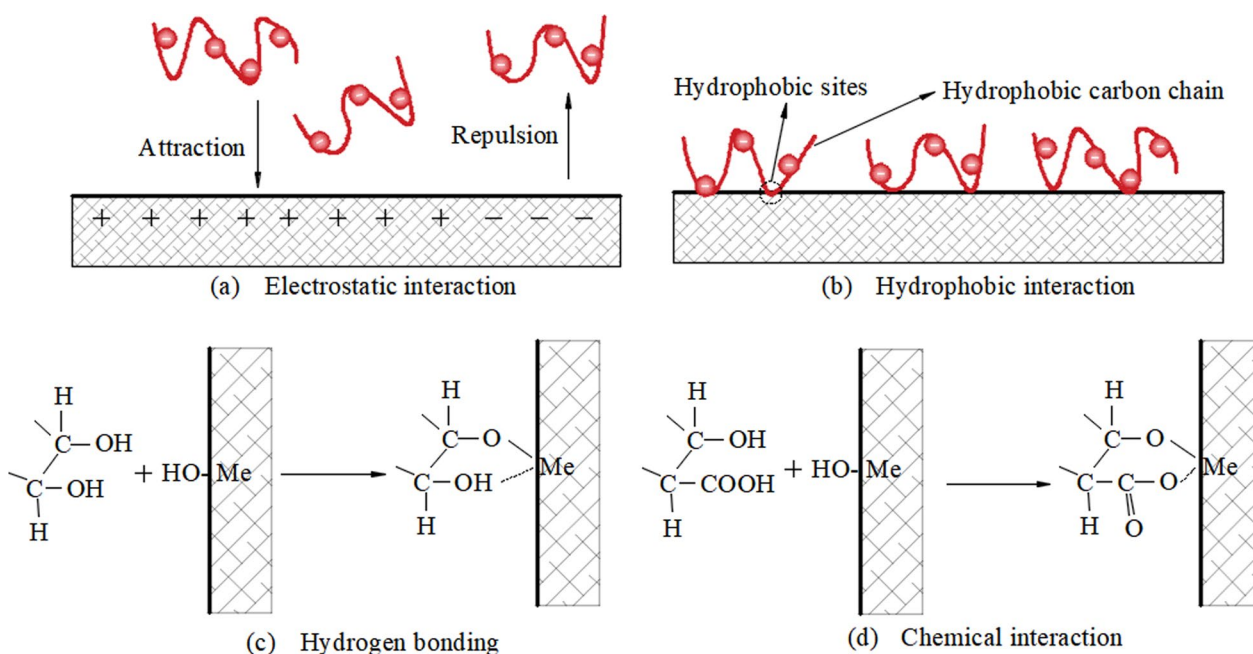

Fig. 7 Possible interaction types between lignosulfonate and pyrite. Modified with permission from Mu et al. (2015)
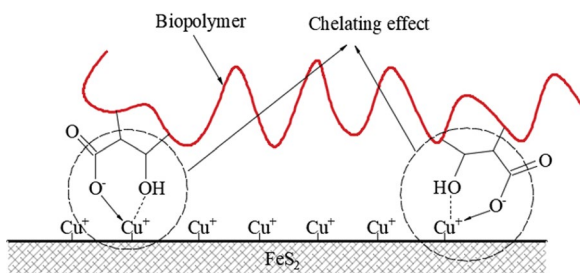
Fig. 8 Chelation between biopolymers and Cu(I) sites on pyrite surface. Modified with permission from Mu et al. (2016c)

is better than that of ionic and covalent metal salts. For instance, 2-mercaptobenzothiazole (MBT) molecule was observed to chelate with metal ions through the thioamide group (Mu et al. 2016a). Six-membered rings were formed due to the chelation between carboxyl, hydroxyl groups, and Cu(I) sites on copper-activated pyrite surface (Fig. 8) (Mu et al. 2016c).

To depress pyrite more effectively during the flotation separation of Cu–S, Khoso et al. (2019a) designed and synthesized a modified biopolymer inhibitor, tricarboxylate sodium starch (TCSS). Flotation results showed that the recovery of Cu was over 77%, and the grade of Cu increased from the initial feed of 12.50% to 24.50%. In addition, because of the weak TCSS/chalcopyrite interaction, the adsorption of xanthate on chalcopyrite surface was limited in the presence of TCSS.

On the other hand, TA is a nontoxic and biodegradable mixture composed of polyphenol substances (Xu et al. 2019). Han et al. (2020a) reported that the Fe atoms on pyrite surface are capable of bonding with the Ph–O and COO⁻ polar groups of TA. The concentration of hydrophilic Fe(III)–O/OH substances increased by 25.75% and 23.61% after pyrite was treated with lactic acid and salicylic acid, respectively. In addition, the hydroxyl groups present in the two molecules also prevented the adsorption of xanthate (Han et al. 2019a, 2020b).

Khoso et al. (2019b) evaluated PGA to separate chalcopyrite from pyrite. The recoveries of chalcopyrite and pyrite were above 85% and below 20% at pH 9, respectively. However, flotation results of actual minerals might differ from those of pure minerals and artificially mixed minerals owing to the atomic doping and monomer dissociation degree of minerals. Therefore, further studies are required in this field to verify the depression effects of PGA in actual ore flotation.

In the search for alternative organic depressants, it was also found that electrochemical characteristics of reagents and minerals are important parameters for their reactivity. Chen et al. (2000a) reported that the electrostatic potential (ESP) of sulfide minerals decreased when TGA was used.

The concentration of dixanthogen decreased when the ESP of sulfide minerals was lower than the reversible potential ($E_{X-/X2}$) of xanthate to dixanthogen. Besides, the reduction of dixanthogen is also controlled by the electronic energy level of mineral, whereas an increase in the Fermi level or a decrease in the edge energy level of sulfide minerals can promote the reduction of dixanthogen. For example, TGA and sodium fulvate initiated the reduction of dixanthogen via increasing the Fermi level and decreasing the edge energy level of pyrite (Chen et al. 2000b).
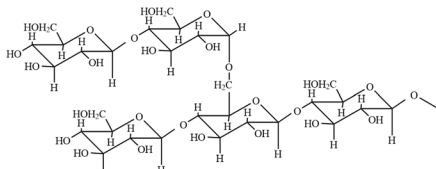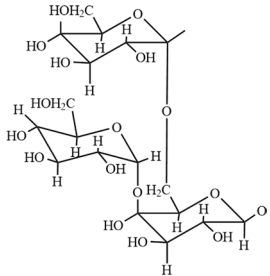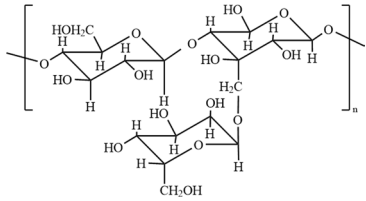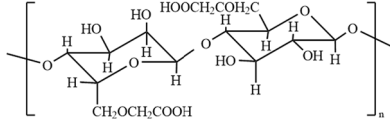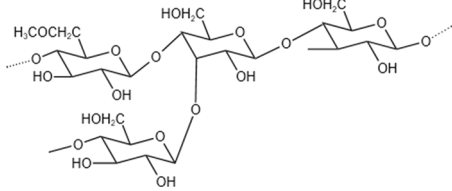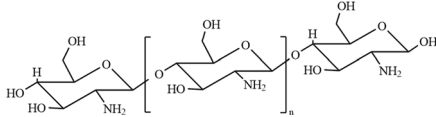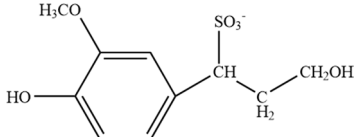
NaA is extracted from weathered lignite and exhibits excellent chemical and electrochemical properties (Cheng et al. 2019b). Chen et al. (2011) reported that the zeta potential and contact angle of pyrite decreased with the addition of NaA, indicating that the hydrophilicity of pyrite improved due to the adsorption of A⁻ ions. Besides, owing to its excellent electrochemical activity (Chen et al. 2000b), the peak position of C–C bond in benzene shifted upon the adsorption of A⁻, demonstrating that chemical adsorption occurred between pyrite and the benzene ring of NaA (Chen et al. 2011).

The characteristics of several typical organic depressants including their toxicity, inhibitory ability, and adsorption methods are shown in Table 2.

4 Effects of Ca²⁺ on the depression of pyrite

The affinity between depressants and minerals is affected by divalent cations such as Ca^{2+} and Mg^{2+} (Chen et al. 2011; Lummer and Plank 2012). Electrostatic repulsion exists between anionic polyelectrolytes and negatively charged solid surfaces, while divalent cations acted as a bridge to drive the adsorption of carboxylate groups on the negatively charged solid surface (Gregory and Barany 2011). For instance, Ca^{2+} increased the electrostatic attraction between polymers and minerals by altering the charge of mineral surface. Negatively charged hydrophilic groups of polymer were neutralized by Ca^{2+}, thus reducing its electrostatic repulsion with polymers (Nanthakumar et al. 2010). $Ca(OH)^+$ formed in the solution might transfer electrons, leading to electron accumulation on pyrite surface that prevented the oxidation of xanthate ions into dixanthogen (Mu et al. 2016c; Zhang et al. 2011). In addition, $Ca(OH)^+$ and Ca^{2+} also reacted with carboxyl groups to promote the adsorption of CMC (Wang 2006). Xiong et al. (2020) and Wang (2013) reported that hydrophilic $CaSO_4$, $Fe(OH)_2$, $Fe(OH)_3$, and $Ca(OH)_2$ precipitates were formed after CaO was dissolved. $Ca(OH)_2$ provided adsorption sites for polysaccharides, leading to the formation of hydrogen bonds between polysaccharides and hydroxyl groups (Bicak et al. 2007). Li et al. (2012) simulated the

Table 2 Characteristics of typical organic depressants

Organic depressant type	Molecular structure	Characteristic
Starch		Nontoxic, abundant reserves, but unsatisfactory inhibiting ability (Liu and Laskowski 1989)
Dextrin		Stronger adsorption capacity on oxidized pyrite surface or surface doped with metal ions (Valdivieso et al. 2004)
Guar gum		Hydrogen bond is the main adsorption form on pyrite (Liu and Laskowski 1989)
CMC		The molecular weight and presence of Ca^{2+} ions affect the inhibitory activity of CMC (Liu and Laskowski 1989)
Konjac glucomannan		The inhibiting activity of konjac glucomannan on pyrite is better than those of starch, dextrin, and guar gum (Liu et al. 2020a)
Chitosan		The adsorption capacity of chitosan depends on the electron affinity of metal ions present on the mineral (Vold et al. 2003)
Lignosulfonate		The functional groups of lignosulfonate are diverse and exhibit good adsorption capacity on pyrite surface (Ouyang et al. 2006)

adsorption of OH^- and $CaOH^+$ on pyrite surface; the Fe–O atomic distances of pyrite and OH^- (1.843 Å) were smaller than those of pyrite and $CaOH^+$ (2.092 Å). Moreover, the electron overlap degree between the O of OH^- and Fe was higher than the electron overlap degree between the O of $CaOH^+$ and Fe. However, the adsorption energy of OH^- on pyrite (− 264.99 kJ/mol) was greater than that of $CaOH^+$ (− 276.62 kJ/mol), and this result is inconsistent to the

conclusions obtained from atomic distance and electron density. Thus, it is believed that Ca^{2+} ions enhanced the interaction between $CaOH^+$ and pyrite. In summary, Ca^{2+} ions promote the adsorption of macromolecules on the surface of minerals and improve the hydrophilicity of minerals, mainly because Ca^{2+} and its hydrolyzed products, $CaOH^+$ and $Ca(OH)_2$, decrease the electrostatic repulsion between polymers and minerals.

5 Quantum chemistry calculations of flotation reagents and molecular simulations of pyrite/reagent interaction

The basic principles of quantum mechanics are applied by utilizing quantum chemistry to evaluate chemical issues at the molecular and atomic levels. From the static perspective, the chemical issues focus on the relationship between structure and properties, while from the dynamic perspective, the interaction and reaction among molecules are involved (Wang 2006). As the fundamental equation of quantum chemistry, Schrödinger's equation is exceptionally complex. The establishment of density functional theory (DFT) is a theoretical leap to overcome this complexity. On the other hand, wave function is regarded as the main physical quantity of a system in traditional quantum theory. Currently, electron density is used in DFT to describe the physical properties of the ground state of a system, simplifying the complex 3 N-dimensional wave function problem into a three-dimensional particle density problem, thus providing a powerful tool to solve quantum chemistry problems (Li et al. 2005). The microscopic morphology and electronic structural changes obtained by DFT provide in-depth studies on the adsorption mechanism of reagents on mineral surface from the atomic level (Chen et al. 2013).

5.1 Surface properties of sulfide minerals

As mentioned before, different environments result in various surface properties of pyrite; for example, the type and concentration of impurity atoms in ore pyrite and coal pyrite crystals are different. Among them, doping of C atoms is noteworthy (Xian 2013). The changes in the physicochemical properties of sulfide surface lead to differences in the adsorption behavior of small molecules such as O_2 and H_2O on its surface. The oxidation of sulfide ore is affected by the adsorption of O_2, whereas the adsorption of H_2O is directly related to the hydrophilicity/hydrophobicity of mineral surface. DFT and molecular dynamics (MD) simulation provide a possible theoretical basis that describes the lattice defects of sulfide ores and the adsorption of small molecules (such as O_2 and H_2O) on sulfide surfaces at the atomic and electronic levels.

Hung et al. reported the surface relaxation and density of state (DOS) of pyrite (100), (110), (111), (210), (001) surfaces and bulk pyrite (Hung et al. 2002b, 2002a; Cai and Philpott 2004). The (100) surface is more stable than the (110) surface, while the (111) surface is more stable than the (210) surface. These results are consistent with the observed frequency of each crystal plane in natural pyrite. Thus, the (001) surface is a conductor, whereas bulk pyrite is a semiconductor with a band gap of 0.90–0.95 eV. Andersson

et al. (2004) and Stirling et al. (2007) reported that the S defect of pyrite fractured surface can be attributed to a point-defect-like sulfur vacancy. Yu (2013) studied the effects of C atom doping on the electronic structure of pyrite. Ideally, pyrite would have a wide energy band, large fluctuations, high degree of nonlocality, and strong metallicity. However, the DOS showed that the top position of the valence band of band gap is determined by the Fe 3d electrons, whereas the bottom position of the conduction band is determined by the S 3p and Fe 3d electrons. With further increase in carbon doping concentration, the DOS of S 3p and Fe 3d gradually shifted to the direction of low energy, the band gap narrowed, and the Fermi energy level decreased. All of them promoted the electron transfer from anionic reagent to mineral surface. For pyrite, as impurity is beneficial to the adsorption of O_2, whereas for the pyrite containing Co and Ni impurities, O_2 existed in the form of peroxide (Li et al. 2011).

The hydration mechanism of mineral surfaces can be further understood by studying the microscopic adsorption behavior of H_2O on the surface. The main interaction between H_2O and pyrite (FeS_2) is the hybridization between O 2p (H_2O) orbital and Fe 3d (FeS_2) orbital, forming a strong Fe–O covalent bond. Xi et al. (2017) calculated the stable adsorption configuration of H_2O molecules on a pyrite (100) surface. Table 3 shows the adsorption energies of H_2O at various sites of pyrite. Based on the adsorption energy, it was deduced that H_2O was adsorbed at the top low position of S site, vertical to the top Fe site, and parallel to the top Fe site, but it was difficult to be adsorbed at the top high position S. The most stable adsorption configuration of H_2O is parallel to the top Fe site (forming two low site S–H bonds).

Chen et al. (2014b) simulated the difference in the surface relaxation and electronic properties of pyrite and galena (PbS) before and after H_2O adsorption. The adsorption of H_2O molecule on the PbS surface occurred via hydrogen bonding between S and H atoms, while Fe/O interactions occurred on the FeS_2 surface. Notably, the S–H bond energies were weakened by the hydrogen bonds between other

Table 3 Adsorption energy of H_2O on pyrite (100) surface (Xi et al. 2017)

Adsorption site	Adsorption energy (kJ/mol)
Top low position S site	− 11.89
Top high position S site	13.11
Vertical to top Fe site	− 38.01
Parallel to top Fe site (two low position S–H bond)	− 70.12
Parallel to top Fe site (two high-position S–H bond)	− 60.79
Parallel to top Fe site (one high position S–H, one low position S–H)	− 64.51

H$_2$O molecules, resulting in a stronger PbS surface hydrophobicity. At the same time, the activity of O 2p orbital increased by the formation of hydrogen bonds between H$_2$O, which is beneficial to the interaction of O 2p and Fe 3d orbital and the hydrophilicity of FeS$_2$. In addition to Fe sites, S sites were also found to be possible oxidation sites for pyrite, and this was experimentally evidenced, where a part of O$_2$ was incorporated into SO$_4^{2-}$ in the isotope composition (Li et al. 2018).

Compared with ideal pyrite, the valence bond between H$_2$O and pyrite changed from Fe–O to Fe–C–O when pyrite surface was covered with C atoms, while the adsorption of H$_2$O decreased due to the weaker C–O bond energy. The adsorption energy of H$_2$O on pyrite changed from negative to positive upon the addition of S atoms on pyrite surface, and the Fe–O bond was converted to Fe–S–O bond. Therefore, the adsorption of H$_2$O on pyrite surface that contains S atoms was found to be thermodynamically unfeasible (Xi et al. 2019). In addition, both the oxidation ability and reactivity of pyrite increased owing to the presence of C impurity. Compared with pyrite with C atoms substituted for S atoms, the oxidation ability and reactivity of pyrite with C atoms substituted for Fe atoms are stronger, whereas ideal pyrite has weak reactivity (Yu 2013). The above conclusions may provide a reference for further studies in the interface reactions of pyrite.

5.2 Quantum chemistry calculation of flotation reagents

In recent studies, adsorption capacity of reagents and minerals has been found to be related to the hydrophilicity/hydrophobicity and special properties of reagents. Frontier orbital energy (E$_{HOMO}$/E$_{LUMO}$), ESP, and degree of charge transfer are crucial parameters that can be calculated using quantum chemistry methods (Medyanik 2011). All these

parameters can be used to evaluate the reactivity of reagents and minerals.

The adsorption of organic reagents on sulfide ores is an electrochemical process; therefore, the desorption between collectors and sulfide ores could be accelerated by the electron transfer between depressants and sulfide ores (Chen et al. 2000b). According to frontier molecular orbital (FMO) theory, the complexity of electron transfer is determined by frontier orbital energy difference $\Delta E_{HOMO-LUMO}$. In mineral flotation, $\Delta E_{HOMO-LUMO}$ represents the difference between the highest occupied molecular orbital energy (E_{HOMO}) of the organic molecule and the lowest unoccupied molecular orbital energy (E_{LUMO}) of the mineral. The smaller the value of |$\Delta E_{HOMO-LUMO}$|, the more spontaneous the reactions between organic molecules and minerals. As such, the frontier orbital energy difference between depressant (Y) and mineral (MS) (|$\Delta E_{(Y-MS)}$|), collector (X) and mineral (MS) (|$\Delta E_{(X-MS)}$|) could be calculated to identify the competitive adsorption capacity of depressants and collectors (Shen et al. 2001; Andersson et al. 2004). Depressants have stronger adsorption abilities on the mineral surface when the relationship in Eq. (6) is satisfied.

$$\left|DE_{(Y-MS)}\right| \leq \left|DE_{(X-MS)}\right| \tag{6}$$

The |$\Delta E_{(Y-MS)}$| values between mercaptoacetic acid, 4-aminobenzene sulfonic acid, and pyrogallic acid and pyrite are 0.15, 0.05, and 0.21 eV, respectively. All of them are less than the |$\Delta E_{(X-MS)}$| between butyl xanthate and pyrite (0.22 eV), and thus they have substantial inhibiting abilities on pyrite (Bogusz et al. 1997). Xi (2017) calculated the frontier orbital energy of following depressants: mercaptoethanol, mercaptopropanol, mercaptobutanol, mercaptoacetic acid, mercaptopropionic acid, mercaptobutyric acid, thiosalicylic acid, 3-mercaptobenzoic acid, and 4-mercaptobenzoic acid. The activity of these types of depressants (mercaptan
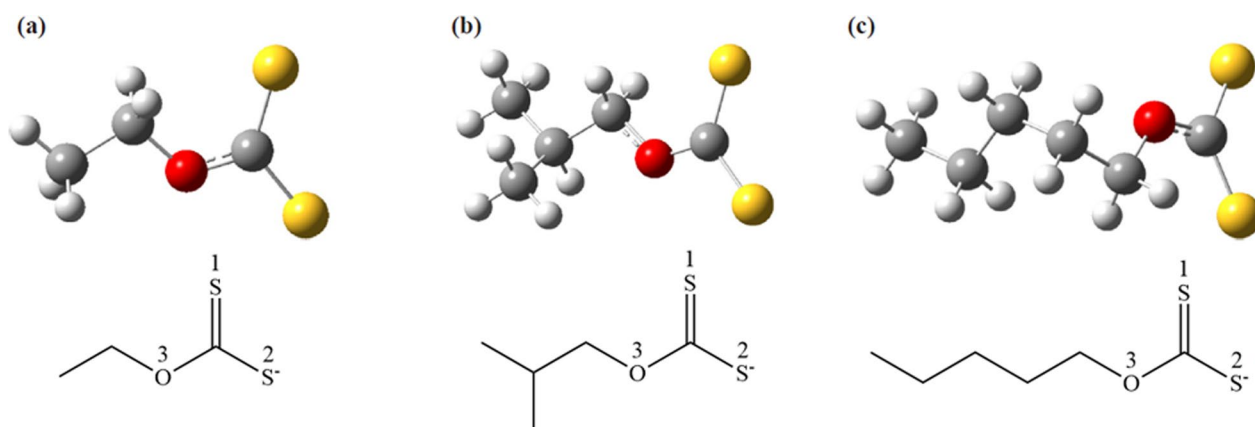

Fig. 9 Most stable configuration of **a** Ethyl xanthate anion, **b** Isobutyl xanthate anion, and **c** Amyl xanthate anion (S = yellow, O = red, C = grey, H = white). Reprinted with permission from Yang et al. (2018)

carboxylic acids and mercaptan alcohols) improved with the increase in carbon chain length. Besides, the reactivity of mercaptan alcohols is stronger than that of mercaptan carboxylic acids when the number of carbon atoms is the same. The HOMO electrons of mercaptan carboxylic acids and mercaptan alcohols were mainly concentrated near the S atoms, whereas the HOMO electrons of mercaptan aromatic carboxylic acids were mainly concentrated near the S atoms and benzene ring. This shows that the S atoms of sulfhydryl groups are the common reactive points for various depressants.

Yang et al. (2018) predicted that the flotation performance of xanthate derivatives with different hydrophobic groups ROC (Fig. 9) decreases in the following order: amyl xanthate > isobutyl xanthate > ethyl xanthate, consistent with the experimental flotation results. In this study, the adsorption of xanthate on the pyrite surface was suggested to be thermodynamically feasible because stable ferric hydroxoxanthate compounds were formed via interactions between xanthate and $Fe(OH)_2^+/Fe(OH)^{2+}$, which subsequently formed hydrophobic layers.

ESP is another important parameter that can be used to predict the interactions between molecules, especially noncovalent bond interactions (e.g., hydrogen bonds). Moreover, the active sites of electrophilic and nucleophilic reactions could be predicted from the ESP of molecules. For example, the areas that correspond to the maximum ESP (such as hydrogen atom in hydroxyl or carboxyl groups) may act as the hydrogen bond donor, while the areas that correspond to the minimum ESP (such as the lone pair of electrons in oxygen-containing functional groups) represent the hydrogen bond receptor. Huang et al. (2019) studied the selective adsorption behavior of S-hydroxyethyl-O-isobutyl xanthate (HEIBX) and sodium isobutyl xanthate (SIBX) for pyrite and chalcopyrite. The ESP values of C=S and OH groups of HEIBX were found to be smaller than those of C=S and C–S groups of SIBX anion, indicating that HEIBX has stronger chemical activity and electron-donating ability than SIBX anion.

The interaction energy between electrophilic molecules and nucleophiles can also be described by electron transfer degree. Medyanik (2011) discovered that the O atoms in carboxyl, hydroxyl, and ester groups are the main nucleophilic centers. Yekeler and Yekeler (2006) studied the electronic properties of MBT, 6-methyl-2-mercaptobenzothiazole, and 6-methoxy-2-mercaptobenzothiazole using DFT calculations at the B3LYP/6-31G(d, p) level. Thioamide group was found to be the active site when MBT molecule bonded with metal atoms. Furthermore, the reactivity of nucleophiles could be improved in the presence of OCH_3 group. Quantum chemistry calculations provide a method to determine the theoretical flotation characteristics of reagents quantitatively, which can provide insights to the selection and design of new flotation reagents.

5.3 Reagents/pyrite interaction

During the flotation, depressants could adsorb and improve the hydrophilicity of targeted minerals. However, competitive adsorption might occur between collectors and depressants on the mineral surface. The equilibrium adsorption configurations of butyl xanthate and isobutyl xanthate at different concentrations on pyrite surface corresponding to constant number, volume, and temperature (NVT), and constant number, volume, and pressure (NPT) ensembles are shown in Figs. 10 and 11 (Han et al. 2018). The hydrophilic head groups of xanthate were found to be adsorbed on pyrite surface, while the alkyl chain extended into the solution. The optimized molecular structures and frontier orbitals of butyl xanthate and isobutyl xanthate are shown in Fig. 12. The HOMO was found to be mainly distributed on the double bond S atom of xanthate molecule, whereas the LUMO was distributed on the hydrophilic group. The ΔE of butyl xanthate and isobutyl xanthate are 3.040 eV and 2.975 eV, respectively, indicating that isobutyl xanthate exhibited better adsorption capacity and surface activity than butyl xanthate, consistent with the experimental results.

Chen et al. (2014a) reported that stronger adsorption occurred between xanthate ions and pyrite with an adsorption energy of -233.35 kJ/mol under anaerobic conditions, while the adsorption energy decreased to -215.19 kJ/mol when oxygen was present, indicating that O_2 is not conducive to the adsorption of xanthate ions on pyrite. Besides, the activity of Fe 3d electrons near the Fermi level decreased after pyrite was oxidized with O_2, weakening the interaction between the oxidized Fe atom and xanthate. The electronic structures of functional groups in hydrogen xanthate, methyl xanthate, and ethyl xanthate were found to be similar. Hung et al. (2003) simulated the adsorption of hydrogen xanthate ion ($HOCS_2^-$) on the defect sites of pyrite surface. When the defect sites (dislocation, S–S bond breakage, etc.) are not oxidized completely, chemical adsorption might occur between the xanthate ions and unoxidized defect sites. However, this process can only occur in an oxygen-free environment because the defect sites of pyrite might be instantaneously oxidized with H_2O and O_2 instead. In a separate study, Chen et al. (2013) reported that the S–Fe distances were smaller than the atomic radius of S–Fe, and the 3d orbital state of Fe atom was closer to the Fermi level (Chen et al. 2014a); therefore, the interaction between xanthate and pyrite was identified to be occurring through the bonding of S and Fe atoms.

Liu et al. (2020b) reported that 6-hexyl-1,2,4,5-tetrazinane-3-thione (HTT) had stronger ability to accept the d-orbital electrons of Cu atoms compared with hexyl xanthate anion, while the weak electron-donating ability of HTT weakened the interaction with Fe atoms. Therefore, HTT would show excellent selectivity in the flotation of chalcopyrite from pyrite.
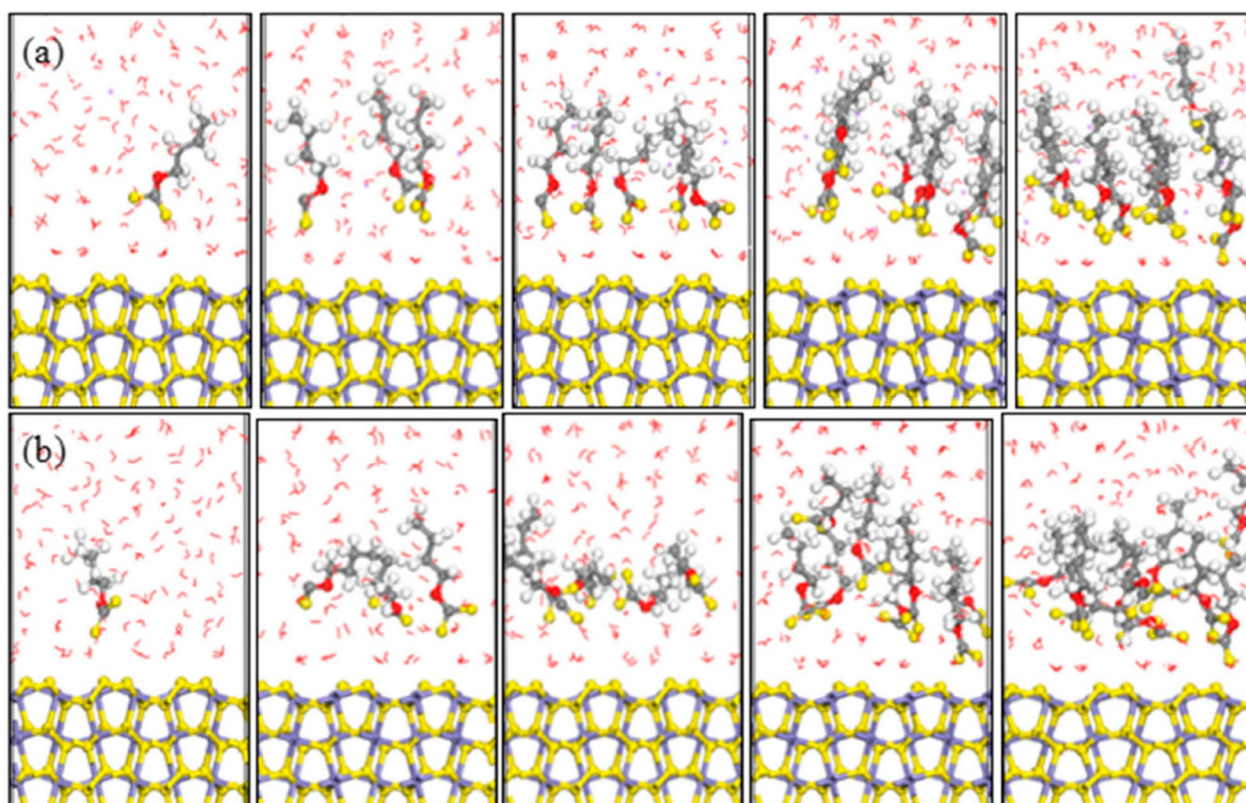
Fig. 10 Equilibrium configurations of different butyl xanthate concentrations on pyrite surface. **a** NVT, **b** NPT (color codes: red=O, white=H, yellow=S, grey=C, iron grey=Fe, purple=Na. The above photographs (from left to right) represent 1, 3, 5, 8, and 10 numbers of xanthate, respectively). Reprinted with permission from Han et al. (2018)

Adsorption energy is also essential to determine the interaction strength between reagents and minerals. Zheng et al. (2018) compared the adsorption configurations of four groups (–SH, –NH$_3$, =O, and –O) of cysteine on pyrite. The most stable adsorption configurations of each group are shown in Fig. 13. The bond lengths of S–S, S–Fe, N–S, N–Fe, O–S, O-Fe, O–S, and O–Fe are 3.027 Å, 2.330 Å, 3.009 Å, 2.176 Å, 3.280 Å, 2.171 Å, 3.018 Å, and 2.155 Å, respectively. As a short bond length depicted strong adsorption capacity, the adsorption abilities of cysteine on Fe atoms were therefore stronger than those on S atoms. It was also noted that chemical adsorption was the main adsorption form of cysteine on the Fe sites.

Niu (2019) observed the formation of FeOOH when pyrite was oxidized with H$_2$O$_2$. To evaluate the effects of oxidation on the adsorption of xanthate, Niu et al. (2019) simulated the interaction between xanthate ions and goethite (FeOOH). The S–Fe distances of xanthate and FeOOH (2.99 Å and 2.80 Å) were larger than the S–Fe distance of xanthate and pyrite (2.284 Å and 2.281 Å), as shown in Fig. 14 (Chen et al.

2013), indicating that the adsorption of xanthate on pyrite surface was stronger than that on FeOOH. As such, the oxidation of pyrite hindered the adsorption of xanthate. Although the Fe atoms of FeS$_2$ and FeOOH were both the adsorption sites of xanthate, different electronic configurations of Fe atoms in the two minerals led to a substantial difference in the adsorption capacity of xanthate (Niu et al. 2019). As shown in Fig. 15, the Fe^{3+} in FeOOH has d^5 high-spin electron configuration, while the Fe^{2+} in FeS$_2$ has d^6 low-spin electron configuration. However, there are 3d vacant orbitals and lone-pair electrons in the 3p orbitals of S atoms for xanthate. The lone-pair electrons of S 3p orbital occupied the e$_g$ empty orbital of Fe atom to form a σ bond when xanthate interacted with pyrite. In addition, a stronger back-bonding π bond formed between the lone-pair electrons donated by the t$_{2g}$ orbitals of Fe atom and the 3d vacant orbital of S atom. However, the high-spin Fe^{3+} ion of FeOOH has neither lone-pair electrons nor empty orbitals. Therefore, σ bonds and back-bonding π bonds were not formed when xanthate was adsorbed on the FeOOH surface (Niu et al. 2019).
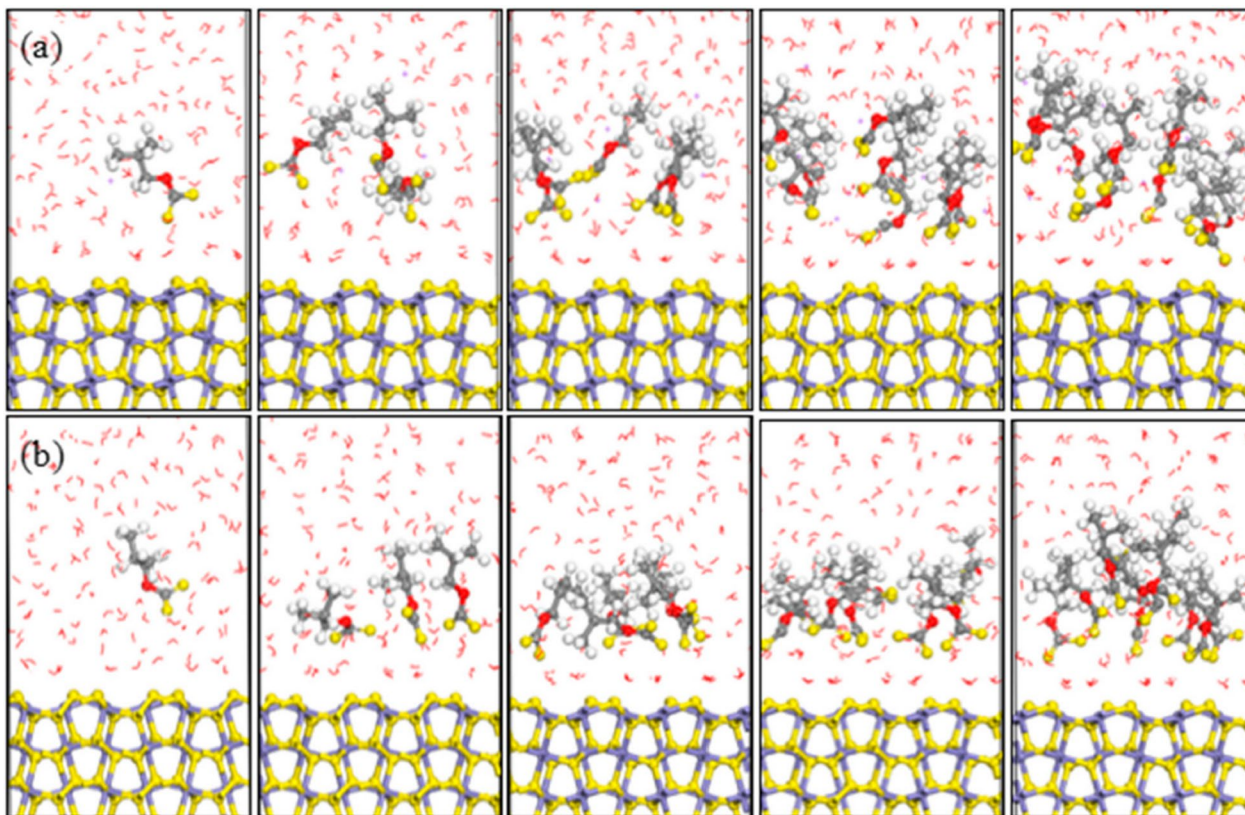
Fig. 11 Equilibrium configurations of different isobutyl xanthate concentrations on pyrite surface. **a** NVT, **b** NPT (color codes: red=O, white=H, yellow=S, grey=C, iron grey=Fe, purple=Na. The above photographs (from left to right) represent 1, 3, 5, 8 and 10 numbers of xanthate, respectively). Reprinted with permission from Han et al. (2018)

Xanthate	Geometric structures	HOMO	LUMO
Butyl xanthate			
Isobutyl xanthate			

Fig. 12 Optimized molecular structures and FMOs of butyl xanthate and isobutyl xanthate (color codes: red=O, yellow=S, white=H, gray=C). Reprinted with permission from Han et al. (2018)

6 Conclusions

With the growing challenges and concerns associated with energy, environment, and social awareness, the mining industry is constantly pressurized to develop smarter, cleaner, and more economical practices. Thus, one of the main research topics in the mining field is the development of flotation desulfurization reagents. For instance, new "green" flotation reagents based on polysaccharide, cellulose, and lignin have been synthesized to replace commonly
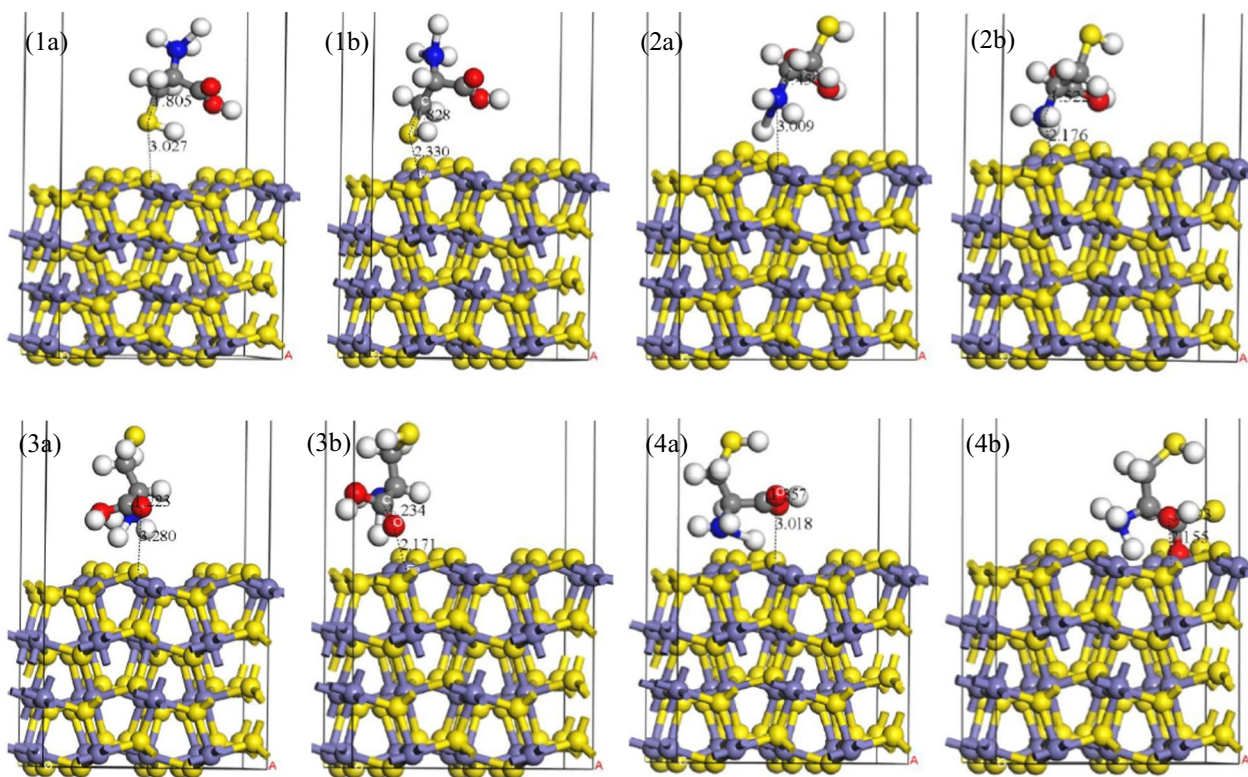
Fig. 13 Optimized configuration of (1) –SH, (2) –NH₃, (3)=O, and (4) –O of cysteine adsorbed on the **a** S site and **b** Fe site of pyrite (100) surface. Reprinted with permission from Zhang et al. (2018)
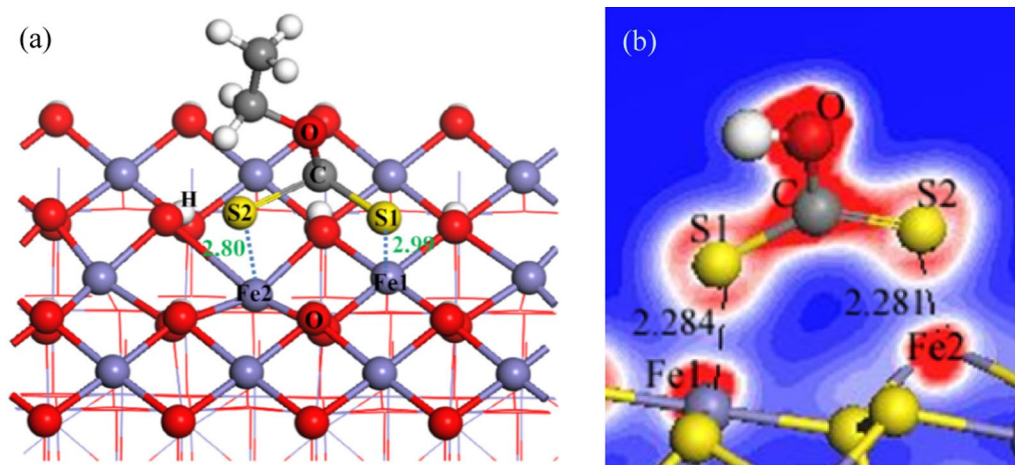

Fig. 14 Optimized configurations of xanthate adsorption on **a** Goethite and **b** Pyrite surface. Reprinted with permission from Niu et al. (2019); Chen et al. (2013)

used nonbiodegradable and chemically harmful reagents. In addition, studies on coal/ore pyrite depressants and their mechanisms, flotation characteristics of depressants, and reagent/mineral interactions have been conducted from the perspective of quantum chemistry and molecular simulation.

Based on this in-depth review, the following problems still need to be addressed in flotation desulfurization:

(1) Foam entrainment and inadequate mineral dissociation mainly affect the flotation desulfurization efficiency. Ongoing and future studies are recommended to focus on optimizing the flotation desulfurization technology.

(2) At present, there are still limited studies on highly efficient flotation reagents. The flotation reagent should be
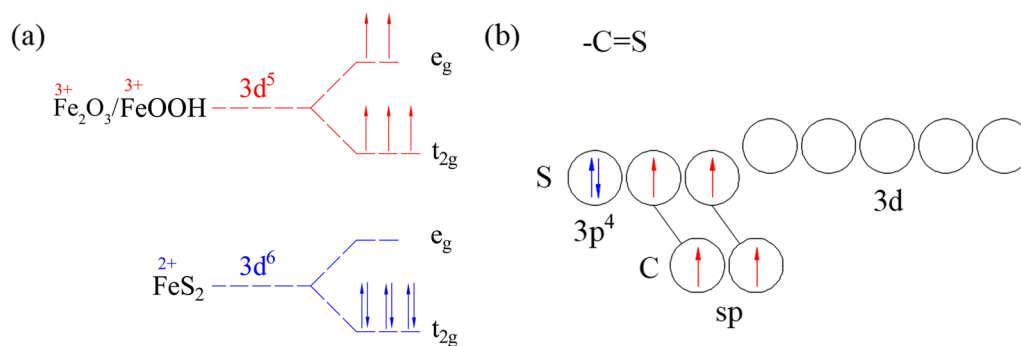
Fig. 15 Valence electron configurations of **a** 3d orbitals of Fe_2O_3, FeOOH, and FeS_2; and **b** –C=S functional group of xanthate. Reprinted with permission from Niu et al. (2019)

"green," highly selective, and have a greater ability to affect the hydrophilicity of target minerals.

(3) While molecular simulation can provide much fundamental information, the results of these simulations are obtained under ideal conditions and may not reflect the experimental results or the actual applications, which are affected by many other external factors. Therefore, the complex surface properties (lattice defects, doping of impurity) of sulfide ore should be reflected in molecular simulation. Besides, the reagent/mineral interaction and particle/bubble interaction are also another key factor that influences the flotation process, which should be included in future simulation studies.

(4) It is also important to note that only a part of the inorganic sulfur can be removed by flotation, while it is difficult to remove the organic sulfur in coal by flotation, which is still an area of research interest.

(5) Finally, although many studies have been conducted in the quantum chemistry and molecular simulation, there are still limited studies on depressants, particularly on pyrite depressants, which is recommended to be further studied.

Declarations

Conflict of interest The authors declare no conflict of interest.

References

Andersson K, Nyberg M, Ogasawara H, Nordlund D, Kendelewicz T, Doyle CS, Brown GE Jr, Pettersson LGM, Nilsson A (2004) Experimental and theoretical characterization of the structure of defects at the pyrite FeS2 (100) surface. Phys Rev B 70:195404

Bai SJ, Yu P, Li CL, Wen SM, Ding Z (2019) Depression of pyrite in a low-alkaline medium with added calcium hypochlorite: experiment, visual MINTEQ models, XPS, and ToF-SIMS studies. Miner Eng 141:105853

Bai SJ, Bi YX, Li J, Yu P, Ding Z, Lv C, Wen SM (2021) Innovative utilization of acid mine drainage (AMD): a promising activator for pyrite flotation once depressed in a high alkali solution (HAS)–gearing towards a cleaner production concept of copper sulfide ore. Miner Eng 170:106997

Bi YX, Pan Y, Ding Z, Bai SJ, Wen SM (2020) The development of research on the pyrite flotation depressants. Conserv Util Miner Res 40:157–166

Bicak O, Ekmekci Z, Bradshaw DJ, Harris PJ (2007) Adsorption of guar gum and CMC on pyrite. Miner Eng 20:996–1002

Bogusz E, Brienne SR, Butler I, Rao SR, Finch JA (1997) Metal ions and dextrin adsorption on pyrite. Miner Eng 10:441–445

Bulut G, Atak S (2002) Role of dixanthogen on pyrite flotation: solubility, adsorption studies and eh. FTIR Meas Miner Metall Proc 19:81–86

Bulut G, Ceylan A, Soylu B, Goktepe F (2011) Role of starch and metabisulphite on pure pyrite and pyritic copper ore flotation. Physicochem Probl Miner Process 48:39–48

Cai J, Philpott MR (2004) Electronic structure of bulk and (001) surface layers of pyrite FeS2. Comp Mater Sci 30:358–363

Cao SM, Cao YJ, Ma ZL, Liao YF (2019) The flotation separation of fine pyrite locked in coking coal. J China Univ Min Technol 48:1366–1374

Chen JH, Feng QM, Lu YP (2000a) Electrochemical mechanism on interaction of TGA with sulphide minerals. Conserv Util Min Resour 6:34–38

Chen JH, Feng QM, Lu YP (2000b) Energy band model of electrochemical flotation and its application (III) - effects of organic depressants on structure of sulphide minerals. Chin J Nonferr Metal 10:529–533

Chen JH, Li YQ, Long QR (2010) Molecular structures and activity of organic depressants for marmatite, jamesonite and pyrite flotation. Trans Nonferr Metal Soc 20:1993–1999

Chen JH, Li YQ, Chen Y (2011) Cu-S flotation separation via the combination of sodium humate and lime in a low pH medium. Miner Eng 24:58–63

Chen JH, Lan LH, Chen Y (2013) Computational simulation of adsorption and thermodynamic study of xanthate, dithiophosphate and dithiocarbamate on galena and pyrite surfaces. Miner Eng 46–47:136–143

Chen JH, Li YQ, Lan LH, Guo J (2014a) Interactions of xanthate with pyrite and galena surfaces in the presence and absence of oxygen. J Ind Eng Chem 20:268–273

Chen JH, Long XH, Chen Y (2014b) Comparison of multilayer water adsorption on the hydrophobic galena (PbS) and hydrophilic pyrite (FeS2) surfaces: a DFT study. J Phys Chem C 118:11657–11665

Cheng G, Zhang CX (2018) Desulfurization and denitrification technologies of coal-fired flue gas. Pol J Environ Stud 27:481–489

Cheng G, Li ZY, Ma ZL, Cao YJ, Sun LJ, Jiang ZD (2019a) Optimization of collector and its action mechanism in lignite flotation. Powder Technol 345:182–189

Cheng G, Niu ZN, Zhang CX, Zhang XM, Li XS (2019b) Extraction of humic acid from lignite by KOH-hydrothermal method. Appl Sci-Basel 9(7):1356

Cheng G, Zhang CX, Zhang XM, Jia K (2019c) Desulfurization of flue gas by means of lignite-derived potassium humate. Fuel 252:646–652

Cheng G, Cao YJ, Zhang CX, Jiang ZD, Yu YX, Mohanty MK (2020a) Application of novel flotation systems to fine coal cleaning. J Coal Prep Util 40:24–36

Cheng G, Li ZY, Cao YJ, Jiang ZD (2020b) Research progress in lignite flotation intensification. Int J Coal Prep Util 40(1):59–76

DeCuir MJ, Gupta RB, Sastri B (2021) Beneficiation of coal using supercritical water and carbon dioxide extraction: sulfur removal. Int J Coal Sci Technol 8:717–726

Ejtemaei M, Nguyen AV (2017) Characterisation of sphalerite and pyrite surfaces activated by copper sulphate. Miner Eng 100:223–232

Fairthorne G, Fornasiero D, Ralston J (1997) Effect of oxidation on the collectorless flotation of chalcopyrite. Int J Miner Process 49:31–48

Feng B, Feng QM, Lu YP, Gu YL (2013) The effect of PAX/CMC addition order on chlorite/pyrite separation. Miner Eng 42:9–12

Fletcher B, Chimonyo W, Peng YJ (2020) A comparison of native starch, oxidized starch and CMC as copper - activated pyrite depressants. Miner Eng 156:106532

Fornasiero D, Ralston J (2006) Effect of surface oxide/hydroxide products on the collectorless flotation of copper-activated sphalerite. Int J Miner Process 78:231–237

Gregory J, Barany S (2011) Adsorption and flocculation by polymers and polymer mixtures. Adv Colloid Interface Sci 169:1–12

Guo B, Peng YJ, Espinosa-Gomez R (2014) Cyanide chemistry and its effect on mineral flotation. Miner Eng 66–68:25–32

Guo B, Peng YJ, Parker G (2016) Electrochemical and spectroscopic studies of pyrite - cyanide interactions in relation to the depression of pyrite flotation. Miner Eng 92:78–85

Han GH, Su SP, Huang YF, Peng WJ, Cao YJ, Liu JT (2018) An insight into flotation chemistry of pyrite with isomeric xanthates: a combined experimentaland computational study. Minerals 8:166

Han G, Wen SM, Wang H, Feng QC (2019a) Lactic acid as selective depressant for flotation separation of chalcopyrite from pyrite and its depression mechanism. J Mol Liq 296:111774

Han G, Wen SM, Wang H, Feng QH (2019b) Effect of starch on surface properties of pyrite and chalcopyrite and its response to flotation separation at low alkalinity. Miner Eng 143:106015

Han G, Wen SM, Wang H, Feng QC (2020a) Interaction mechanism of tannic acid with pyrite surfaces and its response to flotation separation of chalcopyrite from pyrite in a low-alkaline medium. J Mater Res Technol 9:4421–4430

Han G, Wen SM, Wang H, Feng QC (2020b) Selective adsorption mechanism of salicylic acid on pyrite surfaces and its application in flotation separation of chalcopyrite from pyrite. Sep Purif Technol 240:116650

Huang P, Cao ML, Liu Q (2013) Selective depression of pyrite with chitosan in Pb-Fe sulfide flotation. Miner Eng 46–47:45–51

Huang XP, Huang KH, Jia Y, Wang S, Cao ZF, Zhong H (2019) Investigating the selectivity of a xanthate derivative for the flotation separation of chalcopyrite from pyrite. Chem Eng Sci 205:220–229

Hung A, Muscat J, Yarovsky I, Russo SP (2002a) Density-functional theory studies of pyrite FeS2 (111) and (210) surfaces. Surf Sci 520:111–119

Hung A, Muscat J, Yarovsky I, Russo SP (2002b) Density-functional theory studies of pyrite FeS2(100) and (110) surfaces. Surf Sci 513:511–524

Hung A, Yarovsky I, Russo SP (2003) Density-functional theory studies of xanthate adsorption on the pyrite FeS2 (110) and (111) surfaces. J Chem Phys 118:6022–6029

Jha KT, Satur J, Hiroyoshi N, Ito M, Tsunekawa M (2008) Carrier-microencapsulation using Si-catechol complex for suppressing pyrite flotability. Miner Eng 21:889–893

Jha KT, Satur J, Hiroyoshi N, Ito M, Tsunekawa M (2011) Suppression of flotability of pyrite in coal processing by carrier microencapsulation. Fuel Process Technol 92:1032–1036

Jin JQ, Miller JD, Dang LX, Wick CD (2015) Effect of surface oxidation on interfacial water structure at a pyrite (100) surface as studied by molecular dynamics simulation. Int J Miner Process 139:64–76

Khoso SA, Hu YH, Liu RQ, Tian MJ, Sun W, Gao Y, Han HS, Gao ZY (2019a) Selective depression of pyrite with a novel functionally modified biopolymer in a Cu–Fe flotation system. Miner Eng 135:55–63

Khoso SA, Hu YH, Lyu F, Liu RQ, Sun W (2019b) Selective separation of chalcopyrite from pyrite with a novel non-hazardous biodegradable depressant. J Clean Prod 232:888–897

Laskowski JS, Liu Q, O'Connor CT (2007) Current understanding of the mechanism of polysaccharide adsorption at the mineral/aqueous solution interface. Int J Miner Process 84:59–68

Li ZY, He W, Yang JL (2005) Recent progress in density functional theory and its numerical methods. Prog Chem 17:192–202

Li YQ, Chen JH, Guo J (2011) DFT study of influences of As, Co and Ni impurities on pyrite (100) surface oxidation by O2 molecule. Chem Phys Lett 511:389–392

Li YQ, Chen JH, Kang D, Guo J (2012) Depression of pyrite in alkaline medium and its subsequent activation by copper. Miner Eng 26:64–69

Li YQ, Chen JH, Chen Y, Zhao CH, Zhang YB, Ke BL (2018) Interactions of oxygen and water molecules with pyrite surface: a new insight. Langmuir 34:1941–1952

Li YJ, Xia WC, Peng YL, Li YF, Xie GY (2020) Effect of ultrafine kaolinite particles on the flotation behavior of coking coal. Int J Coal Sci Technol 7(3):623–632

Liu Q, Laskowski JS (1989) The interactions between dextrin and metal hydroxides in aqueous solutions. J Colloid Interface Sci 130:101–111

Liu S, Wu Y (2015) Effects of pyrite depressor on high-sulfur coal flotation. Clean Coal Technol 21:40–43

Liu Y, Zhou F (2016) Geological feature and ore genesis for the tuanbaoshan pb-zn deposit in Hanyuan, Sichuan. Sichuan Nonferr Met 4:27–30

Liu Q, Zhang YH, Laskowski JS (2000) The adsorption of polysaccharides onto mineral surfaces: an acid/base interaction. Int J Miner Process 60:229–245

Liu RQ, Sun W, Hu YH, Wang DZ (2009) Effect of organic depressant lignosulfonate calcium on separation of chalcopyrite from pyrite. J Cent South Univ Technol 16:753–757

Liu DZ, Zhang GF, Chen YF, Huang GH, Gao YW (2020a) Investigations on the utilization of konjac glucomannan in the flotation separation of chalcopyrite from pyrite. Miner Eng 145:106098

Liu J, Liu GY, Yang XL, Dong Y, Zhang ZY (2020b) 6-Hexyl-1,2,4,5-tetrazinane-3-thione: flotation selectivity and mechanism to copper sulfide mineral. Miner Eng 152:106345

Lummer NR, Plank J (2012) Combination of lignosulfonate and AMPS®-co-NNDMA water retention agent - an example for dual synergistic interaction between admixtures in cement. Cem Concr Res 42:728–735

Medyanik NL (2011) Quantum chemical descriptors and the assessment of surface activity in coal flotation. Coal 54:103–107

Mu YF, Peng YJ, Lauten RA (2015) Electrochemistry aspects of pyrite in the presence of potassium amyl xanthate and a lignosulfonate-based biopolymer depressant. Electrochim Acta 174:133–142

Mu YF, Peng YJ, Lauten RA (2016a) The depression of copper-activated pyrite in flotation by biopolymers with different compositions. Miner Eng 96–97:113–122

Mu YF, Peng YJ, Lauten RA (2016b) The depression of pyrite in selective flotation by different reagent systems—a literature review. Miner Eng 96–97:143–156

Mu YF, Peng YJ, Lauten RA (2016c) The mechanism of pyrite depression at acidic pH by lignosulfonate-based biopolymers with different molecular compositions. Miner Eng 92:37–46

Nanthakumar B, Arinaitwe E, Pawlik M (2010) Adsorption of sodium lignosulfonates on hematite. Adsorption 16:447–455

Niu XP (2019) Correlation of surface oxidation of galena, chalcopyrite and pyrite with their flotability. University of Chinese Academy of Sciences, Beijing

Niu XP, Chen JH, Li YQ, Xia LY, Li L, Sun HY, Ruan RM (2019) Correlation of surface oxidation with xanthate adsorption and pyrite flotation. Appl Surf Sci 495:143411

Ouyang XP, Qiu XQ, Chen P (2006) Physicochemical characterization of calcium lignosulfonate—a potentially useful water reducer. Coll Surf A 282–283:489–497

Ouyang XP, Zhang P, Tan CM, Deng YH, Yang DJ, Qiu XQ (2010) Isolation of Lignosulfonate with Low Polydispersity Index. Chin Chem Lett 21:1479–1481

Pecina ET, Camacho LF, Herrera CA, Martínez D (2012) Effect of complexing agents in the desulphurization of coal by H2SO4 and H2O2 leaching. Miner Eng 29:121–123

Qi X, Zhang HJ, Zhang CQ, Zhu ZN, Zhen KK, Yang L (2019) The flotation behavior of coal-pyrite in high-sulfur coal. Sep Sci Technol 54:2718–2728

Rath RK, Subramanian S, Pradeep T (2000) Surface chemical studies on pyrite in the presence of polysaccharide-based flotation depressants. J Coll Interface Sci 229:82–91

Sarquís PE, Menendez-Aguado JM, Mahamud MM, Dzioba R (2014) Tannins: the organic depressants alternative in selective flotation of sulfides. J Clean Prod 84:723–726

Satur J, Hiroyoshi N, Tsunekawa M, Ito M, Okamoto H (2007) Carrier-microencapsulation for preventing pyrite oxidation. Int J Miner Process 83:116–124

Shao XX, Tang YG, Wang PF (1994) The ESCA study of coal pyrite and pyrite. Anal Util Coal Qual 2:9–18

Shao XX, Ren SZ, Li J, Zhang JH (1997) Desulfurization of fine coal by flotation method. J China Coal Soc 22:182–186

Shen WZ, Fornasiero D, Ralston J (2001) Flotation of sphalerite and pyrite in the presence of sodium sulfite. Int J Miner Process 63:17–28

Shi XP, Zhu H, Ou ZS (1997) Effect of coal pyrite surface oxidation on coal desulfuration by flotation and methods of pyrite depression. J Wuhan Univ Technol 12:37–41

Sotillo FJ, Fuerstenau DW, Harris GH (1997) Surface chemistry and rheology of pittsburgh no. 8 coal-water slurry in the presence of a new pyrite depressant. Coal Prep 18:151–83

Stirling A, Bernasconi M, Parrinello M (2007) Defective pyrite (100) surface: an Ab initio study. Phys Rev B 75:165406

Sun W, Liu RQ, Hu YH (2005) Research on depression mechanism of jamesonite and pyrrhotite by organic depressant DMPS. Min Metall Eng 25:31–34

Tang YG, He X, Cheng AG, Li WW, Deng XJ, Wei Q, Li L (2015) Occurrence and sedimentary control of sulfur in coals of China. J China Coal Soc 40:1977–1988

Tao XX, Xu N, Xie MH, Tang LF (2014) Progress of the technique of coal microwave desulfurization. Int J Coal Sci Technol 1:113–128

Tu ZH (2017) Studies of sulfur transformation in oxidation of pyrite and surface electrochemistry of pyrite oxidation. South China University of Technology, Changsha

Valdivieso AL, Cervantes TC, Song S, Cabrera AR, Laskowski JS (2004) Dextrin as a nontoxic depressant for pyrite in flotation with xanthates as collector. Miner Eng 17:1001–1006

Valdivieso AL, López AAS, Song S (2005) On the cathodic reaction coupled with the oxidation of xanthates at the pyrite/aqueous solution interface. Int J Miner Process 77:154–164

Valdivieso AL, López AAS, Song S, Martínez HAG, Almada SL (2007) Dextrin as a regulator for the selective flotation of chalcopyrite, galena and pyrite. Can Metall Q 46:301–309

Vold IMN, Vårum KM, Guibal E, Smidsrød O (2003) Binding of ions to chitosan-selectivity studies. Carbohyd Polym 54:471–477

Wang BJ (2006) Study on quantum chemistry of coal structure and reactivity. Taiyuan University of Technology, Taiyuan

Wang QF (2013) Research on desulphurization and deashing for medium-high sulphur coal with flotation. Qingdao University of Technology, Qingdao

Wang XH, Forssberg KSE (1991) Mechanisms of pyrite flotation with xanthates. Int J Miner Process 33:275–290

Wang XH, Forssberg KSE (1996) The solution electrochemistry of sulfide-xanthate-cyanide systems in sulfide mineral flotation. Miner Eng 9:527–546

Wang P, Zhou Q, Du YS, Yu WC, Xu Y, Qi L, Yuan LJ (2016) Characteristics of pyrite sulfur isotope of Mn deposit from Datangpo formation in Songtao area, East Guizhou Province and Its geological significance. Earth Sci 41:2031–2040

Xi P (2017) Quantum chemistry investigation on the physicochemical property of coal pyrite and its inhibitory regularities. China University of Mining and Technology, Beijing

Xi P, Liu WL, Han YH, Chen JH, Song CZ (2016) Study on the mechanism of coal pyrite crystal lattice defects and flotability. J China Coal Soc 41:997–1003

Xi P, Wang DH, Liu WL, Shi CS (2019) DFT study into the influence of carbon material on the hydrophobicity of a coal pyrite surface. Molecules 24:3534

Xian YJ (2013) Study on crystal defects and surface adsorption characteristics of pyrite. Kunming University of Science and Technology, Kunming

Xiong MJ, Huang YT, Fu JG, Zhao D, Wang XB (2020) Study on deashing, desulfurization and upgrading of high sulfur coal by deep - flotation combined with chemical oxidation. Clean Coal Technol 26:64–71

Xu L (2018) Comparative study on physicochemical properties of coal and non-coal minerals (kaolinite and pyrite) - a case study of late paleozoic coal in Datong. China University of Mining and Technology, Xuzhou

Xu WH, Han EH, Wang ZY (2019) Effect of tannic acid on corrosion behavior of carbon steel in NaCl solution. J Mater Sci Technol 35:64–75

Xu YL, Liu Y, Bu YC, Chen ML, Wang LY (2021) Review on the ionic liquids affecting the desulfurization of coal by chemical agents. J Clean Prod 284:124788

Yang XL, Albijanic B, Liu GY, Zhou Y (2018) Structure-activity relationship of xanthates with different hydrophobic groups in the flotation of pyrite. Miner Eng 125:155–164

Yekeler H, Yekeler M (2006) Predicting the efficiencies of 2-mercapto-benzothiazole collectors used as chelating agents in flotation processes: a density-functional study. J Mol Model 12:763–768

Yin WZ, Yang B, Fu YF, Chu FD, Yao J, Cao SH, Zhu ZL (2019) Effect of calcium hypochlorite on flotation separation of covellite and pyrite. Powder Technol 343:578–585

Yu JX (2013) Study on the physical and chemical characteristics of coal—pyrite and its inhibitors. China University of Mining and Technology, Xuzhou

Zhang Y, Qin WL, Sun W, He GY (2011) Electrochemical behaviors of pyrite flotation using lime and sodium hydroxide as depressantors. Chin J Nonferr Metal 21:675–679

Zhao CH, Huang DW, Chen JH, Li YQ, Chen Y, Li WZ (2016) The interaction of cyanide with pyrite, Marcasite and Pyrrhotite. Miner Eng 95:131–137

Zheng XF, Pan X, Nie ZY, Yang Y, Liu LZ, Yang HY, Xia JL (2018) Combined DFT and xps investigation of cysteine adsorption on the pyrite (100) surface. Minerals 8:366

Zhu YM, Jia JW, Ma YW, Gao P, Han YX, Zhao JJ, Li JB (2013) Adsorption of sodium cyanide on pyrite particle surface. Adv Mater Res 826:3–9